

PHASE I FINAL REPORT

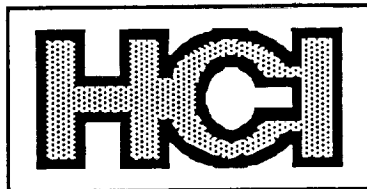
NAS 9-17740

METAL HYDRIDE
THERMAL MANAGEMENT
TECHNIQUES FOR
FUTURE SPACECRAFT
AND
PLANETARY BASES

AUGUST, 1987

PREPARED FOR

THERMAL SYSTEMS BRANCH
CREW AND THERMAL SYSTEMS DIVISION
NATIONAL AERONAUTICS AND SPACE ADMINISTRATION
LYNDON B. JOHNSON SPACE CENTER
HOUSTON, TEXAS



HYDROGEN CONSULTANTS, INC.
12420 N. DIAMOND WAY, LITTLETON, CO 80125

(NASA-CR-190993) METAL HYDRIDE
THERMAL MANAGEMENT TECHNIQUES FOR
FUTURE SPACECRAFT AND PLANETARY
BASES, PHASE I Final Report
(Hydrogen Consultants) 75 p

N93-70015

Unclass

29/54 0127430

1. The first part of the document is a list of names and addresses of the members of the committee.

2. The second part of the document is a list of names and addresses of the members of the committee.

3. The third part of the document is a list of names and addresses of the members of the committee.

4. The fourth part of the document is a list of names and addresses of the members of the committee.

5. The fifth part of the document is a list of names and addresses of the members of the committee.

6. The sixth part of the document is a list of names and addresses of the members of the committee.

7. The seventh part of the document is a list of names and addresses of the members of the committee.

8. The eighth part of the document is a list of names and addresses of the members of the committee.

9. The ninth part of the document is a list of names and addresses of the members of the committee.

10. The tenth part of the document is a list of names and addresses of the members of the committee.

PHASE I FINAL REPORT

NAS 9-17740

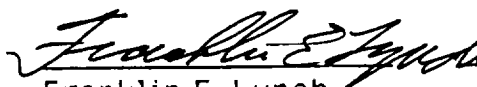
METAL HYDRIDE
THERMAL MANAGEMENT
TECHNIQUES FOR
FUTURE SPACECRAFT
AND
PLANETARY BASES

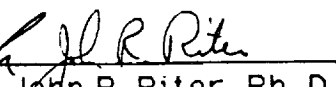
AUGUST, 1987


PREPARED FOR

THERMAL SYSTEMS BRANCH
CREW AND THERMAL SYSTEMS DIVISION

NATIONAL AERONAUTICS AND SPACE ADMINISTRATION
LYNDON B. JOHNSON SPACE CENTER
HOUSTON, TEXAS


Franklin E. Lynch
Principal Investigator


John R. Riter, Ph. D.
Senior Chemist


Susan Wittman
Research Engineer



HYDROGEN CONSULTANTS, INC.
12420 N. DUMONT WAY, LITTLETON, CO 80125
(303) 794-7972

ABSTRACT

Future space missions will encounter a range of challenging thermal environments. Long mission durations, great distances and infrequent resupply intervals will limit previous approaches to thermal control that consume Earth resources. The establishment of lunar and Martian bases presents opportunities for thermal management in new ways occasioned by the availability of high quality waste heat from nuclear power systems and the ability to reject heat to subsurface rock or, on Mars, to the atmosphere. Metal hydrides can serve in future thermal control systems by pumping, storing and transmitting thermal energy with minimal consumption of electricity. Hydrides are lightweight, compact, nonventing two-phase media which enable unique thermally powered methods of heat pumping, thermal storage, and transmission of thermal energy over long distances. The Phase I study identified several beneficial uses for hydrides in future thermal management systems including:

- Auxiliary cooling for spacecraft prior to departure from LEO
- Heat pumping and thermal buffering at bases with hydrides from local mineral resources
- Compact thermal control for EMU's and rovers
- Acquiring thermal power at a remote nuclear power system and transmitting it to a safe distance for use in thermal management
- Synergistic use of hydride thermal control devices for hydrogen storage or for shielding from nuclear, solar and cosmic radiation.

TABLE OF CONTENTS

SECTION	SUBJECT	PAGE
1.0	Introduction	1-1
2.0	Metal Hydrides In Thermal Control Systems	2-1
3.0	Heat Sources and Sinks In Future Space Missions	3-1
3.1	Heat Sources for Hydride Thermal Subsystems	3-1
3.2	Environmental Conditions	3-5
3.3	Conduction of Heat into Subsurface Rock	3-14
4.0	Hydride Applications In Future Space Thermal Systems	4-1
4.1	LEO Thermal Accessory	4-2
4.2	Hydride Cooler Based on Lunar Materials	4-7
4.3	Hydrides and Mobility	4-12
4.4	Hydride Heat Pipes	4-15
4.5	Synergism Between Hydrides and Other Subsystems	4-17
5.0	Summary and Conclusions	5-1
6.0	References	6-1
Appendix A	Computer Simulation Methods	A-1
A.1	References for Appendix A	A-5

LIST OF FIGURES

FIGURE	SUBJECT	PAGE
2-1	H ₂ pressures over metal hydrides and vapor pressures over liquids	2-3
2-2	LaNi ₅ H ₆ absorption/desorption hysteresis band	2-3
2-3	Pressure vs. hydrogen content isotherm for LaNi ₅ -hydride	2-4
2-4	Metal hydride thermal storage cycle	2-6
2-5	Schematic of a metal hydride refrigerator	2-7
2-6	Thermally powered refrigeration cycle	2-8
2-7	Thermodynamic sketch of a hydride heat pump	2-10
2-8	Flow schematic of a hydride heat pump	2-11
3-1	Solar thermal sources in Earth or Moon orbits	3-2
3-2	Solar thermal sources in Mars orbit	3-2
3-3	Thermal optimization of the SP-100	3-4
3-4	CO ₂ pressure-enthalpy diagram & refrigeration cycle	3-13
3-5	Radiator performance at the surface of Mars' moons	3-14
3-6	General concept for a Mars Drilling Rig	3-15
3-7	Subsurface rock heat exchanger	3-16
3-8	Rock conduction model	3-17
3-9	Rock temperature profile	3-18
3-10	Temperature vs. time in a basalt heat sink	3-19

LIST OF FIGURES (cont'd)

FIGURE	SUBJECT	PAGE
4-1	LEO thermal accessory	4-4
4-2	Heat flow in a hydride heat pump	4-5
4-3	Equilibrium pressure-temperature diagram	4-6
4-4	Waste heat from a nuclear thermoelectric generator	4-9
4-5	Metallic cooling cycle	4-10
4-6	Major components of a MHHP	4-13
4-7	Heat pump cycle	4-14
4-8	Rover	4-14
4-9	Remote hydride heat pump	4-16
4-10	Hydride H ₂ /heat buffer	4-18
4-11	Active thermal control subsystem	4-21
A-1	Cutaway view of the hydride tube model	A-2
A-2	Computer model flow diagram	A-3

LIST OF TABLES

TABLE	SUBJECT	PAGE
1-I	Properties of phase change materials for thermal control	1-4
2-I	Thermodynamic properties of typical hydrides	2-5
3-I	Nominal solar, reflected & infrared fluxes in low orbits	3-6
3-II	Major constituents of the Martian atmosphere	3-8
3-III	Martian planetary surface atmospheric transport	3-9
3-IV	Convective heat transfer coefficients on Mars	3-11
4-I	Comparison of metal hydrides	4-20

1.0 INTRODUCTION

This is the Phase I final report on Contract NAS 9-17740, "Metal Hydride Thermal Management Techniques for Future Spacecraft and Planetary Bases". The Small Business Innovation Research study was conducted by Hydrogen Consultants, Inc. of Denver, Colorado for the Thermal Systems Branch of the Crew and Thermal Systems Division, Lyndon B. Johnson Space Center (JSC), Houston, Texas. JSC's Technical Manager was Melaine Sedej. The purpose of the study was to evaluate the potential use of hydride-based thermal control subsystems at lunar or planetary bases, and in advanced spacecraft associated with these future space activities.

Future space exploration activities are likely to include the establishment of a permanently inhabited base on the Moon (Mendell ed., 1985) and manned expeditions to Mars and its moons, Phobos and Deimos (NASA, 1986; Duke and Keaton eds., 1986). This study will be limited to lunar and Martian activities to keep the scope within the bounds of a Phase I SBIR contract. However, the curiosity of humans about their surroundings must eventually be extended to the entire solar system and beyond. The most challenging thermal control applications arise in manned missions because of the narrow range of temperatures within which humans can work in comfort. To maintain the health and productivity of crews during the long duration of future space activities, an effective and reliable thermal control system is essential.

Metal hydrides have been identified as promising materials for Space Station thermal control applications including refrigeration (Egan and Lynch 1985), heat pumping and thermal storage (Lynch and Riter 1987). These metal-hydrogen compounds absorb, store and release more heat per unit of volume than alternative materials. The working fluid, hydrogen, offers *commonality* with cryogenic propulsion, fuel cells, lunar materials processes and advanced environmental control systems. Hydride heat pumps and refrigerators operate by simple thermodynamic relationships with no complex mechanical equipment. Unlike two-phase fluids, their operation is not affected by gravity or the lack of it.

One of the features of metal hydride subsystems that makes them particularly well suited for applications in future spacecraft and planetary bases is their ability to use thermal power in lieu of electricity. Solar thermal nuclear or fuel cell waste heat can power active thermal control devices, conserving electric power for other purposes. The only electrical power requirements are for fluid circulation and control.

The future space activities that are the subject of this study are in the early planning stages, and many details which affect the design of thermal control systems are not settled at this time. However, it is clear that there will be significant differences between the thermal systems of the Space Station and previous spacecraft compared to those of lunar and planetary bases and associated vehicles. Nuclear power systems, such as the SP-100, are envisioned in a number of future space applications (Buden and Angelo, 1984; J. French, 1984; Colston, 1986). This will provide megawatts of thermal energy at temperatures that are more than adequate to power metal hydride thermal cycles.

Spacecraft that provide transportation and support for future space missions must also have advanced thermal systems to cope with a much broader range of operating conditions than in any previous manned mission. During preparation for departure, the thermal systems of these vehicles must operate in the cyclic insolation of low earth orbit (LEO, ca. 90 minute). Then, enroute to any destination more distant than the Moon, the environmental conditions change significantly because solar intensity varies as the square of distance from the Sun. After arrival at a planet or a moon an orbit will be established, probably with an orbital period different from low earth orbit, so a new cyclic thermal environment is encountered. The size of the crew may change at this time as some crewmembers depart to the surface in a lander. This has a direct impact on the metabolic input to the spacecraft thermal system, and indirectly affects other heat loads.

The thermal systems of landers also offer significant challenges. A lander on the Earth's Moon will encounter a significant range of conditions that (except for polar sites) will vary with the diurnal cycle. During the two-week lunar day, surface temperatures rise to 405 K (270°F). Surface temperatures fall to 105 K (-270°F) during the two-week lunar night (B. French, 1977). Mars landers will also experience large environmental variations that are dependent on time of day (sol), latitude, altitude, and the Martian seasons. Maximum daytime temperatures of 240 K (-28°F) and minimum nighttime temperatures of 190 K (-118°F) are typical of the two Viking lander sites (Kllore, ed., 1982). In addition to the temperature variations, wind speed and the amount of dust in the atmosphere will affect the thermal environment of a Mars lander. Mars' moons, Phobos and Deimos, are small and cold compared to Earth's moon. Rapid changes in insolation occur during the short orbital periods of these moons (7.65 hrs. and 30.3 hrs. respectively). Surface structures and vehicles must also contend with these thermal environments.

Perhaps the most versatile thermal control systems of all will be those of the extravehicular mobility units (EMUs). It may be most efficient in terms of mass and volume to have only one type of EMU aboard during lunar or planetary missions. In that case, the thermal control system would need to function in LEO before departure, in varying space environments during transit, and on the surface after arrival.

In addition to the radiators commonly used onboard spacecraft, a lunar base thermal system may conduct heat to lunar soil or rock. A Martian base may also reject heat by conduction into the surface or by convection to the Martian atmosphere. The atmosphere of Mars, with its clouds and frequent dust storms, will impact the design of radiators. The Martian atmosphere also provides a limitless source of CO_2 . In its solid or liquid states, CO_2 could be useful as a working fluid and as a storage medium in thermal control subsystems (Waligora and Sedej, 1986).

Raw materials for manufacturing metal hydrides are abundant in lunar minerals such as ilmenite (Taylor, 1975). Viking soil samples also indicate the presence of useful minerals at Mars (Gornitz, ed., 1979). There is considerable support for the idea of producing oxygen from lunar ilmenite (Mendell, ed., 1985). Ilmenite contains iron and titanium in the correct proportions to manufacture FeTi, an alloy that reacts with hydrogen to form FeTiH_2 . If oxygen is to be produced from ilmenite, the mining, beneficiation, and some of the energy and processing required to manufacture FeTi could be written off against oxygen production. FeTi would be a by-product, gained through a marginal expenditure of energy. The point of relevance to thermal system planning is that hydrides, for use at a growth phase lunar base, may not need to be transported from Earth. Table 1-1 compares selected hydrides to other thermal storage media in terms of heat stored per unit of mass and volume. It is noteworthy that few of the alternatives could conceivably be manufactured from lunar resources.

The balance of this report will discuss

- how metal hydrides interact with heat sources and heat sinks in thermal control systems in general,
- what environmental conditions are likely to impact thermal system performance at future lunar and planetary bases and associated vehicles,
- and where metal hydrides look promising for these future missions.

Table 1-1. Properties of phase change materials for thermal control.

The endothermic phase changes are indicated by heat arrows (Δ) between the initial and final phases; G = 1 atm. gas, G* = gas @ P other than 1 atm., L = liquid, S = solid and S* indicates a new solid phase. The last column lists the latent heat per unit volume, sometimes called the *volumetric energy density*. It is the product of the preceding two columns, density x latent heat per unit mass (*gravimetric energy density*).

Substance	Phase Change	Temp °C	kg/m ³	x MJ/kg = MJ/m ³	
Hydrated Eutectic Salt	S Δ L	7	1500	0.126	189
Glauber's Salt	S Δ L	32	1460	0.251	366
Ice	S Δ L	0	910	0.333	303
n-Hexadecane	S Δ L	17	770	0.238	183
Pentaerythritol	S Δ S*	189	1390	0.303	421
Neopentyl Alcohol	S Δ S*	-31	810	0.053	43
HYDRIDES (two are required)					
FeTi Monohydride	S Δ S* + G	-8	5470	0.134	733
Rare Earth Ni ₅ Hexahydride	S Δ S* + G	-40	5800	0.172	998
Vanadium Dihydride	S Δ S* + G	21	4800	0.356	1709
Magnesium Dihydride	S Δ S* + G	286	1450	2.845	4125
VENTING ALTERNATIVES (e.g., Mars, Phobos, ...)					
Water, 8×10^{-3} atm	L Δ G*	5	1000	2.488	2488
Ice, 10^{-3} atm	S Δ G*	-20	920	2.836	2609
Carbon Dioxide, 8×10^{-3} atm	S Δ G*	-123	1620	0.598	969
Carbon Dioxide, 39 atm	L Δ G*	5	895	0.216	193

2.0 METAL HYDRIDES IN THERMAL CONTROL SYSTEMS

Future spacecraft and planetary bases will require advanced thermal control systems to manage heat loads of unprecedented magnitude and unusual types. The special properties of metal hydrides permit novel thermal control processes that are not possible with other phase-change materials. On a mass basis, metal hydrides can absorb and release as much heat as the best alternative phase change materials, such as salts or paraffins. On a volume basis hydrides are superior. The properties of several phase-change materials are compared to metal hydrides in Table 1-1 above. Hydrides also offer unique operational advantages that make them attractive candidates for future space thermal systems:

- Hydrides can be configured in pairs, consisting of two different metal compositions with vastly different hydride transformation temperatures. This feature--impossible with other phase-change materials--facilitates unique types of heat pumps, refrigerators and heat pipes.
- The gaseous phase, hydrogen, can only "condense" inside the hydride containers where the powdered metal is stored--no problems with zero-g liquid acquisition or unintentional condensation in transfer lines at the lowest temperatures encountered aboard spacecraft.
- The phase change is controllable by adjustment of the hydrogen flow into or out of the hydride, thus permitting more precise temperature regulation than alternative materials.
- Hydride subsystems can be maintained indefinitely in the space environment because the hydride materials are not volatile, except for hydrogen gas which can be replenished from other sub-systems (propulsion, ECLSS, etc.).

Metal hydrides are chemical compounds formed by reactions between solid metals (usually powders) and hydrogen gas. Hydrogen exists within the metal hydride crystal structure as interstitial atoms. As hydrogen is absorbed and released, a phase change with a large latent heat occurs. Metallurgists often concern themselves with the differences between the two solid phases--metal and metal hydride. It is more useful, for the purposes at hand, to focus on the

behavior of the hydrogen as it transforms from gas to solid and back again. Either point of view indicates a phase-change with a latent heat of transformation. Focusing on the hydrogen places the use of hydrides in the familiar realm of liquid-vapor systems, such as steam cycles, cryogenic propellants, and Freon refrigerators.

Figure 2-1 compares the pressure-temperature characteristics of typical metal hydrides with those of vaporizing liquids. These "van't Hoff plots" show that the same relationship is exhibited between absolute pressure and absolute temperature. The hydride data in Figure 2-1 are equilibrium desorption data, indicating the final pressure after extracting a small amount of hydrogen gas at constant temperature. The best hydrides will yield virtually the same data in absorption, when hydrogen is added. The difference between desorption and absorption is called pressure hysteresis, and its effects must be accounted for in the design of hydride devices. A typical hydride hysteresis band is shown in Figure 2-2. The pressure-temperature data points were established by measuring pressure-composition isotherms at 10°C intervals between 25°C and 65°C. A typical pair of absorption/desorption isotherms is shown in Figure 2-3. The horizontal portions of the isotherms ("plateau" pressures) correspond to the 25°C points in Figure 2-2. Metal hydrides may be metallurgically engineered to react with hydrogen at virtually any pressure and temperature.

Hydride equilibrium may be accurately described by equilibrium constants of the form

$$K_p = P_{H_2}$$

for desorption, and

$$K_p = 1/P_{H_2}$$

for absorption, where P_{H_2} is the plateau pressure of the hydride, expressed in atmospheres. With these definitions, standard enthalpy, free energy and entropy (ΔH° , ΔG° and ΔS°) for desorption or absorption processes may be calculated as follows:

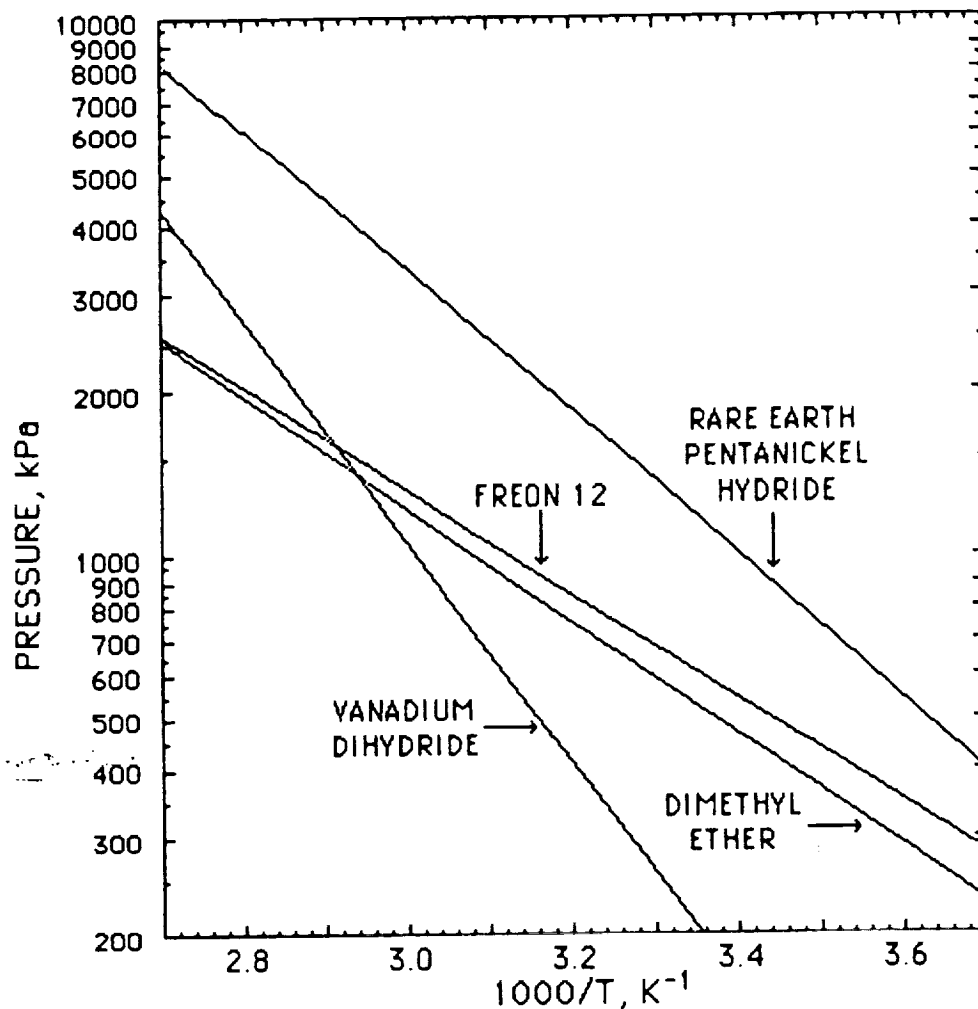


Figure 2-1. Hydrogen pressures over metal hydrides vary in much the same way as vapor pressures over liquids.

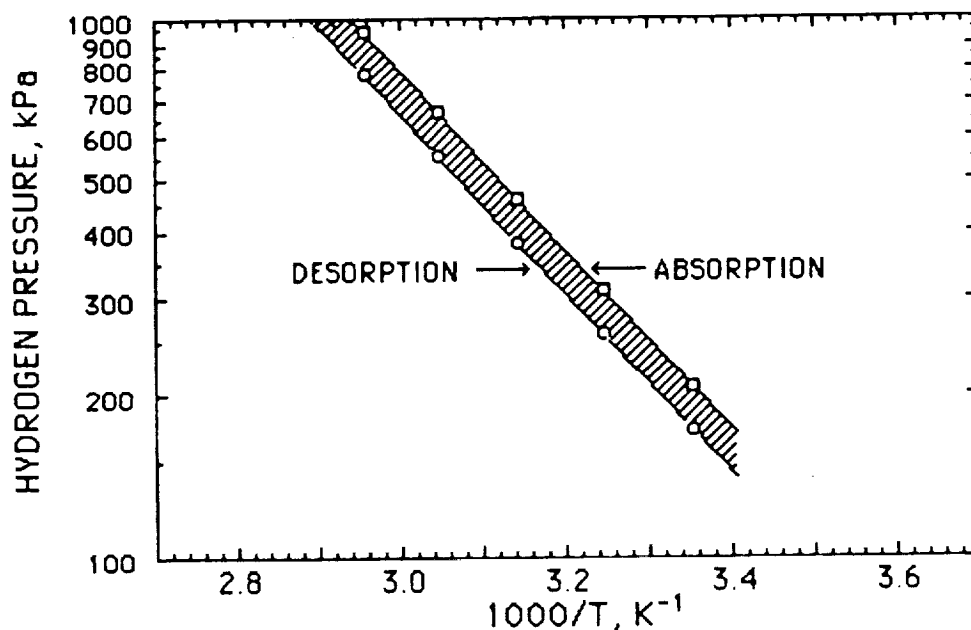


Figure 2-2. $LaNi_5H_6$ (Lundin & Lynch, 1976) shows a typical absorption/desorption hysteresis band.

$$\Delta H^\circ_T = \frac{-R \, d \ln K_p}{d \, 1/T}$$

$$\Delta G^\circ_T = -RT \ln K_p$$

$$\Delta S^\circ_T = \frac{\Delta H^\circ_T - \Delta G^\circ_T}{T}$$

The slopes of hydride van't Hoff plots give the derivatives, $d \ln K_p / d(T^{-1})$, that are needed to determine the enthalpies, ΔH°_T . The absorption lines are parallel to the desorption lines so that, recalling that $K_p = 1/P_{H_2}$, absorption ΔH°_T is the negative of desorption ΔH°_T to a very good approximation. Similar sign changes occur in the calculation of ΔG°_T and ΔS°_T . Calculated values of ΔH° , ΔG° and ΔS° for typical hydrides at 298.15 K are listed in Table 1-1.

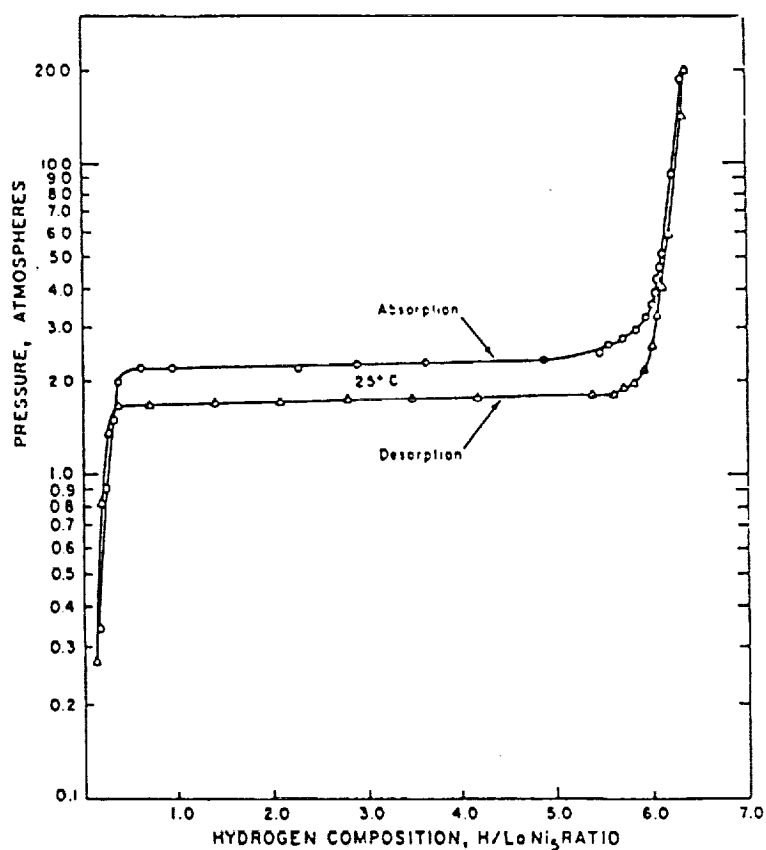


Figure 2-3. Pressure vs. hydrogen content isotherm for LaNi₅-hydride at 25°C. The upper curve is for absorption the lower curve is for desorption (Lundin & Lynch, 1976).

Table 2-1. Thermodynamic properties of typical hydrides.

A = Absorption @ T = 298.15K D = Desorption @ T = 298.15K		ΔH°_T kJ/mol H ₂	ΔG°_T kJ/mol H ₂	ΔS°_T J/mol H ₂ ·K
A	$\frac{1}{3}\text{LaNi}_5 + \text{H}_2 \rightarrow \frac{1}{3}\text{LaNi}_5\text{H}_6$	-30.9	1.5	-108.7
D	$\frac{1}{3}\text{LaNi}_5\text{H}_6 \rightarrow \frac{1}{3}\text{LaNi}_5 + \text{H}_2$	30.9	-1.3	108.0
A	$\frac{1}{3}\text{La}_{0.9}\text{Gd}_{0.1}\text{Ni}_5 + \text{H}_2 \rightarrow \frac{1}{3}\text{La}_{0.9}\text{Gd}_{0.1}\text{H}_6$	-29.2	3.3	-109.0
D	$\frac{1}{3}\text{La}_{0.9}\text{Gd}_{0.1}\text{H}_6 \rightarrow \frac{1}{3}\text{La}_{0.9}\text{Gd}_{0.1} + \text{H}_2$	29.2	-2.9	107.7
A	$2\text{VH} + \text{H}_2 \rightarrow 2\text{VH}_2$	-40.2	1.6	-140.2
D	$2\text{VH}_2 \rightarrow 2\text{VH} + \text{H}_2$	40.2	-0.6	136.8
A	$2\text{FeTi} + \text{H}_2 \rightarrow 2\text{FeTiH}$	-28.1	5.1	-111.4
D	$2\text{FeTiH} \rightarrow 2\text{FeTi} + \text{H}_2$	28.1	-3.5	106.0

In addition to the equilibrium thermodynamics discussed above, metal hydride absorption/desorption processes are affected by dynamic factors, including chemical kinetics and heat transfer. HCL uses a proprietary computer model called HAWK (Hydride Analysis With Kinetics) to account for the effects of dynamic factors on the performance of hydrides. The model uses a first-order (diffusion-like) reaction rate equation and a nodal heat transfer simulation to estimate the dynamic performance of realistic metal hydride devices. A typical use of HAWK during this project was to estimate rates of heat pumping cycles. Appendix A contains a detailed discussion of HAWK.

The simplest thermal use of metal hydrides may be for thermal storage. The concept is illustrated in Figure 2-4. A heat source is thermally coupled to hydride A, driving hydrogen out through the valve and into hydride B. Hydride B is cooled by a radiator or other suitable heat sink. There may be a large difference in temperature between hydrides A and B as well as a large

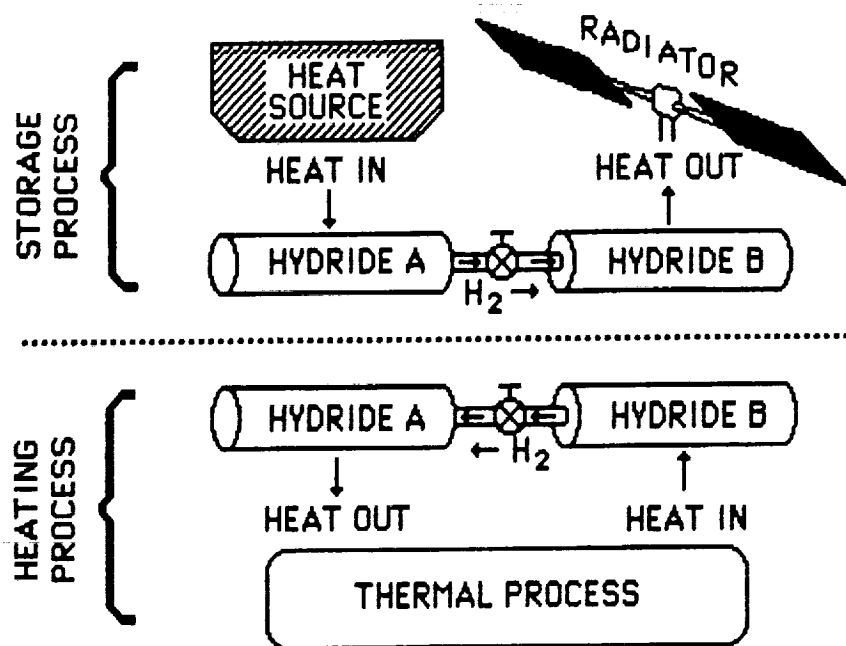


Figure 2-4. Metal hydride thermal storage cycle. The upper half of the figure shows the storage of heat while the lower half shows the subsequent use of stored heat.

difference between the heats of the two reactions. For example, hydride A might be MgH_2 at 450°C , storing 75 kJ/g-mol H_2 desorbed, while hydride B is LaNi_5 at 115°C rejecting only 31 kJ/g-mol H_2 absorbed.

After the hydrogen has all been driven from hydride A to hydride B, the valve between the two hydrides may be closed, storing the chemical potential energy indefinitely. At some later time when heat is needed, the valve may be opened and hydride A will deliver 75 kJ/g-mol H_2 absorbed at a temperature of about 385°C while hydride B consumes 31 kJ/g-mol H_2 desorbed. The heat consumed by hydride B may come from a waste heat stream in the thermal process or, if necessary, from hydride A. The latter case reduces the net available heat to 44 kJ/g-mol H_2 absorbed by hydride A.

If, in the preceding example of thermal storage, hydride B had been coupled to a higher temperature heat source, hydride A could have delivered process heat at temperatures well above 450°C . This is a form of heat pumping that can be accomplished by hydrides. Hydride heat pumping and refrigeration cycles take advantage of the fact that the "vapor" phase, hydrogen, has two different pressure-temperature characteristics in the presence of two different metals. In Figures 2-4 and 2-5, hydrides A and B have differing hydrogen stabilities (standard free energies). If both hydrides are at the same temperature, the equilibrium hydrogen pressure of hydride A is less than the equilibrium hydrogen pressure of hydride B. This pressure difference causes

hydrogen to flow from B to A to minimize the chemical potential energy of the system. This natural tendency for hydrogen to reside in container A can be driven backwards by applying heat to container A. This occurs during the "Recharge Process" depicted in the upper half of Figure 2-5. Heat is converted to chemical potential energy as hydrogen is driven from A into B. During this process heat is rejected from hydride B to the heat sink. When all of the hydrogen has been transferred, the "Refrigeration Process", depicted in the lower half of Figure 2-5, can commence. The stored chemical potential energy is released as hydrogen flows back to its natural state in container A. Hydrogen, desorbing from hydride B, is analogous to evaporation, which extracts heat from the refrigerated zone. Hydrogen, absorbed by hydride A is analogous to condensation and heat is rejected to the heat sink.

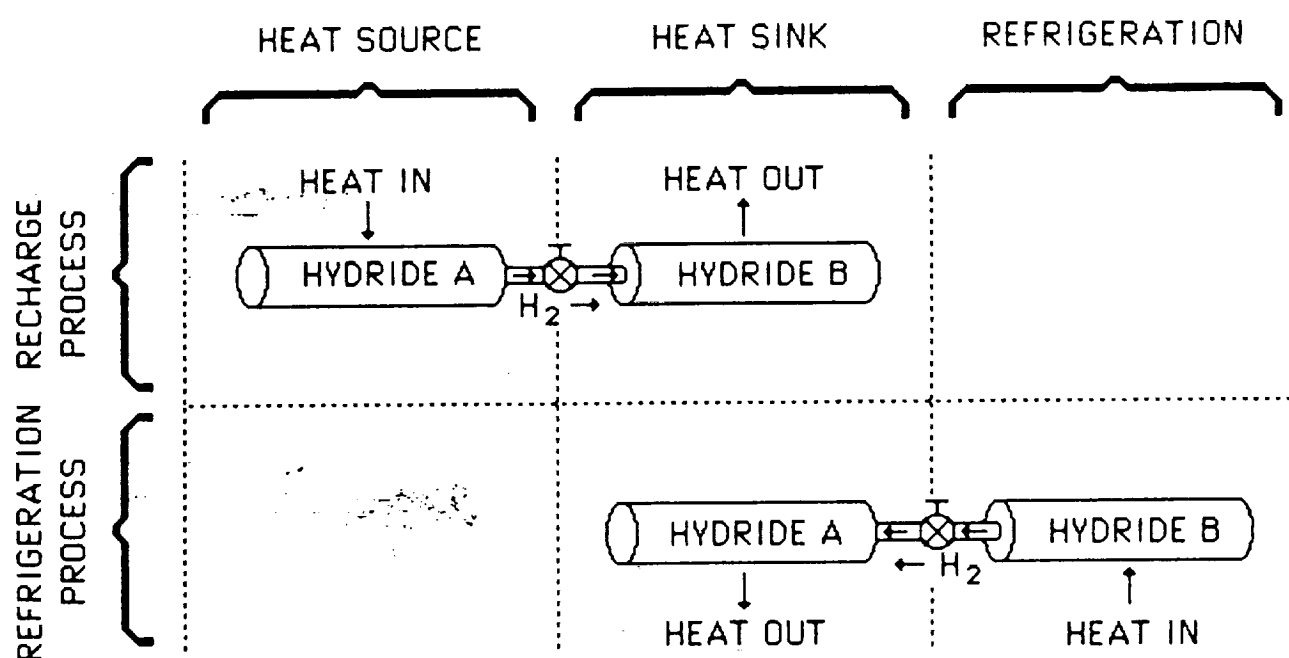


Figure 2-5. Schematic of a metal hydride refrigerator. The figure is divided into three temperature zones--heat source, heat sink, and a refrigerated zone--by the vertical lines. The refrigeration cycle consists of two parts:

Recharge Process:

Hydrogen is driven out of hydride A by heat supplied by the heat source. Hydrogen flows through the tube between the two containers and into hydride B where it is absorbed. The heat of absorption is rejected to the heat sink.

Refrigeration Process:

Hydride B extracts heat from the refrigerated zone as it decomposes endothermically, flowing hydrogen into hydride A. The heat of absorption is rejected from hydride A to the heat sink.

The large heat (ΔH^*) flow during a hydride refrigeration cycle, is related to a change in standard free energy (ΔG^*), temperature (T) and standard entropy (ΔS^*) by Gibbs' Function, $\Delta H^* = \Delta G^* + T\Delta S^*$. In an idealized isothermal phase change, ΔG^* and T are constant so that the heat flow is attributable to ΔS^* . The entropy changes during hydride/dehydride reactions are, in turn, directly related to hydrogen volume changes. In real hydride refrigeration equipment the gas is consumed by one hydride as fast as it is liberated by the other hydride, so there is never any significant volume of gas phase. For the development of thermodynamic insight however, it is useful to imagine that constant pressure accumulators store the hydrogen gas flowing from one hydride and then (after a temperature change) deliver it to the other hydride.

Figure 2-6 traces the volume changes during an idealized hydride refrigeration cycle. The cycle begins at a negligible volume, V_8 (solid phase hydrogen in the hydride), cold temperature (T_c), and low pressure (P_{l0}). Hydride B desorbs a volume (V_1) of hydrogen as it consumes heat (endothermically) at T_c . The gas is warmed from T_c to the sink temperature (T_s) and in the process grows to volume, V_2 . Hydride A rejects heat (exothermically) as it absorbs hydrogen at T_s and P_{l0} . During this step, the hydrogen volume decreases to V_3 , the negligible volume of solid phase hydride A. Hydride A is then heated to T_h as the pressure rises to P_{hi} . The volume, V_4 , remains negligible because

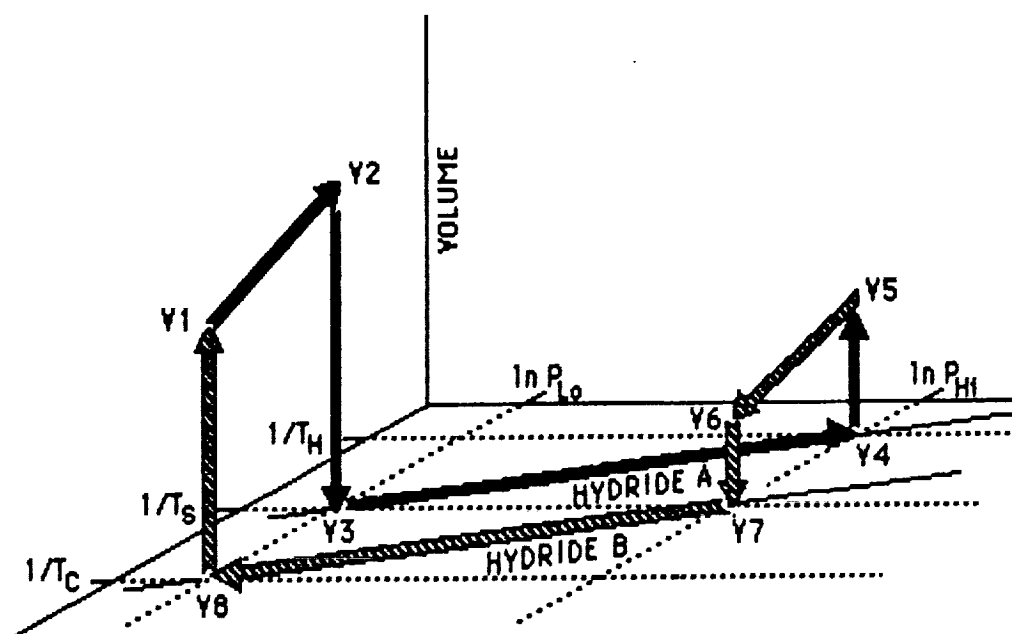


Figure 2-6. Thermally powered refrigeration cycle. The base plane is the van't Hoff plot ($\ln P$ vs. $1/T$). The volumes, V_1 through V_8 , show how the volume of the gas phase, hydrogen, changes during the cycle.

virtually* all of the hydrogen remains in the solid phase during the heating process. At $\ln P_{hi}$ and T_h , hydrogen transforms back to the gaseous phase and volume grows from V_4 to V_5 as hydride A decomposes endothermically. The ratio $V_5/V_2 = (P_{lo}/P_{hi})(T_h/T_s)$, neglecting compressibility. Hydrogen volume then decreases from V_5 to V_6 as the gas phase cools from T_h to T_s . Hydride B rejects heat to the heat sink at T_s as it absorbs hydrogen (exothermically) and volume becomes negligible again as V_6 falls to V_7 . The cycle is closed as hydride B cools to the cold temperature, T_c , equilibrium pressure falls to P_{lo} , and hydrogen volume remains negligible between V_7 and V_8 .

Plots similar to Figure 2-6 could be constructed with other extensive thermodynamic variables, such as enthalpy or entropy, in place of volume. The general appearance and interpretation would be essentially unchanged. Volume changes are easy to visualize as perpendicular to the $\ln P$ vs. $1/T$ plane and thus clarify the thermodynamic details of the process.

Figure 2-6 was drawn with only one heat sink, shared the by A and B hydrides. This is not a necessary condition and, in general, the two hydrides may be placed at different locations and release their heat to two different heat sinks at greatly different temperatures. Figure 2-7 is a schematic of a hydride heat pumping cycle wherein each hydride sheds heat to a separate radiator. The temperatures of the heat source, heat sinks and coolant loop in Figure 2-7 correspond to an example discussed in greater detail in Section 4.2 of this report. Figure 2-7 shows how hydride A acts as a heat engine, consuming heat at a higher temperature and rejecting heat at a lower temperature while doing work in the form of hydrogen compression. Hydride B acts as a heat pump, extracting heat at a low temperature and rejecting it at a higher temperature while consuming work from the compressed hydrogen flow. The heat and hydrogen flows are illustrated as continuous processes for the sake of clarity. These flows are actually pulsed as the hydride pair alternates between absorption and desorption. The work done by A on B is the net result of hydrogen exchange between the two hydrides during a complete cycle. Two A-containers and two B-containers are shown to illustrate the need for two or more hydride pairs to maintain continuous heat pumping.

The preceding discussion of thermally powered hydride heat pumping cycles has dealt with idealized representations of heat input and output between metal hydride containers and their heat sources and heat sinks. Real hydride

*Hydride containers are designed to minimize empty space, which would otherwise allow significant volume changes during the heating process.

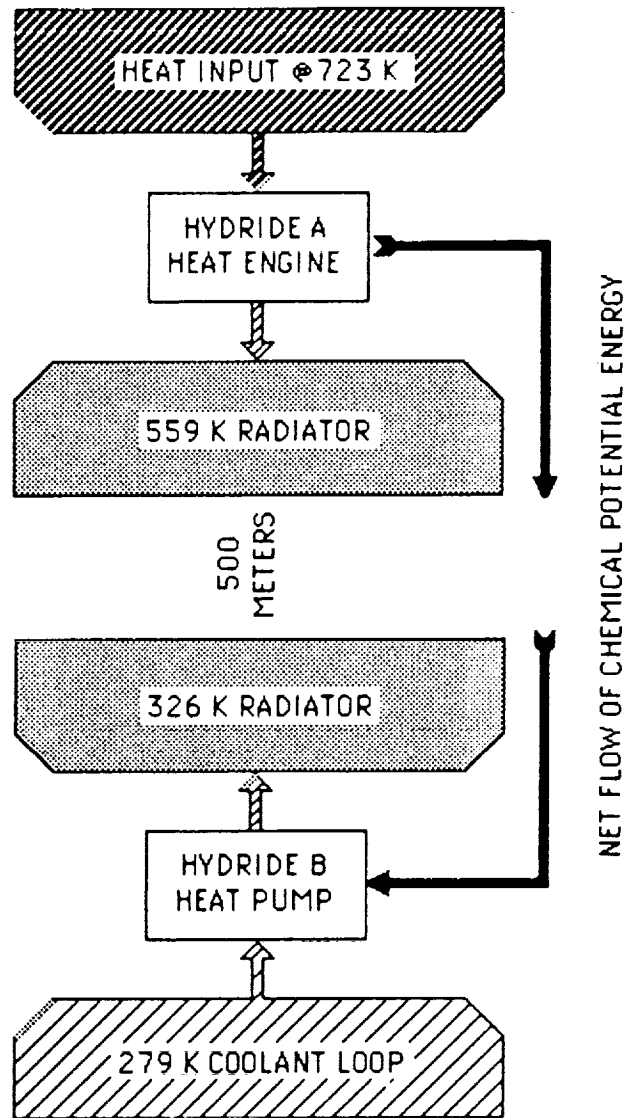


Figure 2-7. Thermodynamic sketch of thermal power transmission from a remote heat source to a hydride heat pump.

containers are often formed from a plurality tubular pressure vessels, bundled together and surrounded by a shell that contains flows of heating/cooling fluid--i.e., tube and shell heat exchangers.

Figure 2-8 shows how two A-B pairs of hydride containers might be arranged in a fluid system to provide a continuous flow of coolant to a manned module. The four-way valves alternate the flow of pumped heat transfer fluids through each pair, A1-B1 and A2-B2, so that one of the two B hydride containers is always connected to the coolant loop in the module. The cooling rate is regulated by flow control valves in the hydrogen lines.

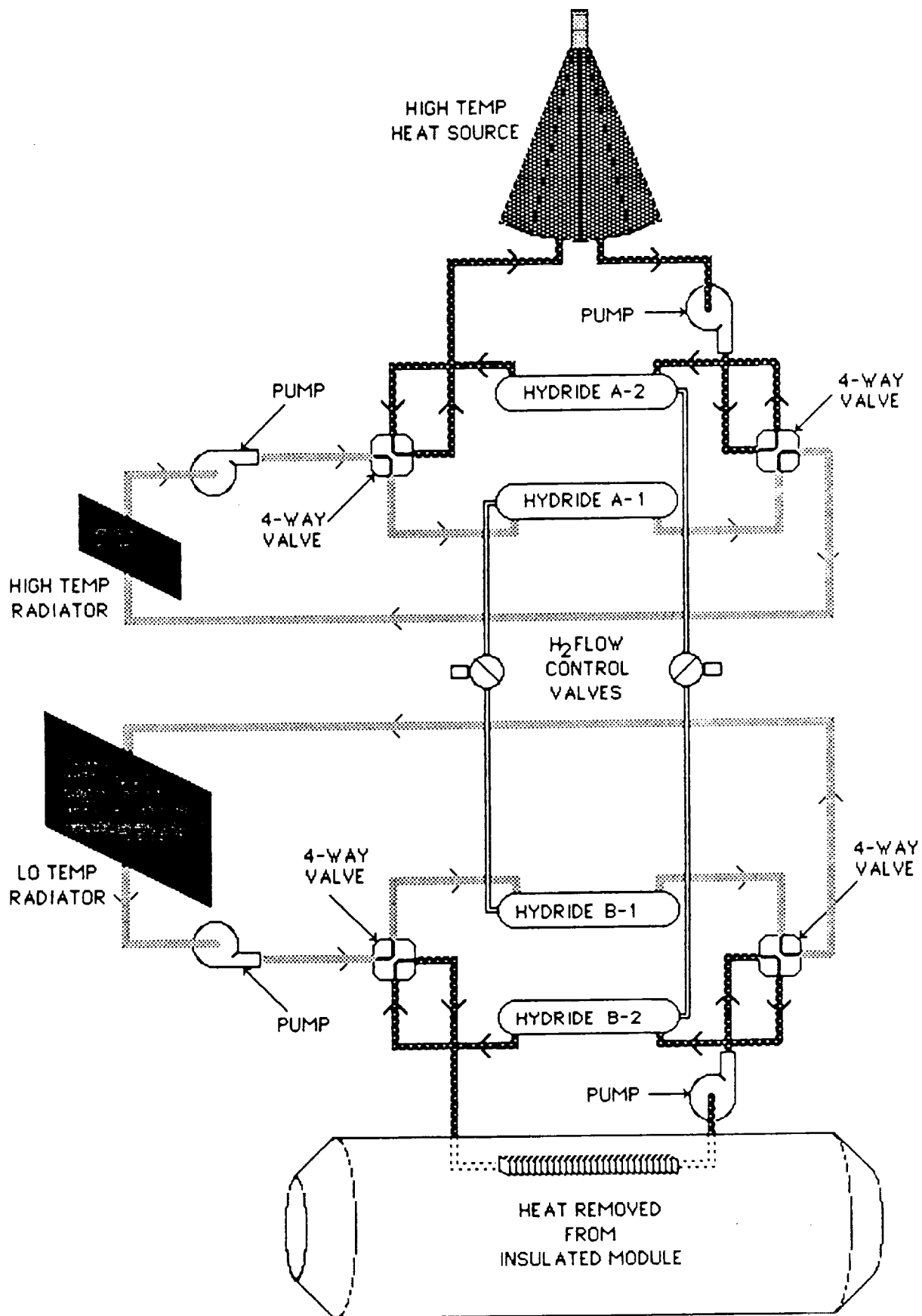


Figure 2-8. Schematic of a thermally powered metal hydride heat pump.

3.0 HEAT SOURCES AND SINKS IN FUTURE SPACE MISSIONS

The performance of metal hydride thermal subsystems is strongly tied to the availability of adequate heat sources and heat sinks. This places several diverse subjects within the scope of this study because they influence the temperatures and heat flows of potential sources and sinks in future spacecraft, lunar and planetary bases, and associated vehicles. Power systems are the primary sources of waste heat to be exploited by hydride devices, so the thermal details of power systems projected for future space missions were examined to determine how they might be interfaced with hydride components in thermal systems. The environment was a major variable in the study because it effects the heat load on thermal systems and the ability of radiators to dissipate heat. Environments of interest included LEO, lunar and Mars orbits, and space travel far from any environmental heat sources other than the Sun. The prospect of surface bases presents some challenging environmental conditions as well as unique opportunities to dissipate heat. Part of the study effort was spent in understanding how metal hydride thermal system components might dissipate heat to rock beneath the surfaces of the Moon and Mars and in characterizing the heat transfer properties of the Martian atmosphere.

3.1 HEAT SOURCES FOR HYDRIDE THERMAL SUBSYSTEMS

A variety of power systems are under consideration for use in future space activities. Solar dynamic power cycles or photovoltaics may be particularly useful at either a polar lunar base or a transportation depot located at a libration point, because the Sun is virtually always in sight. Planar (flat plate) photovoltaic power systems do not offer easy access to the waste heat shed from the back sides of the panels. Concentrating photovoltaics could be designed to dissipate heat to heat exchangers that provide thermal power to metal hydride devices.

It may be desirable, in some circumstances, to collect solar thermal heat for the purpose of operating metal hydride thermal devices. Lower temperature hydride applications may be served by planar arrays or simple body mounted collectors. This might include the regeneration of EMU heat pumps with thermal energy in the neighborhood of 400 K. Other hydride thermal subsystems will need higher temperatures, from steerable solar concentrators. Figures 3-1 and 3-2 show the estimated performance of solar thermal collectors in Earth-Moon and Mars orbits (1352 W/m^2 and 583 W/m^2

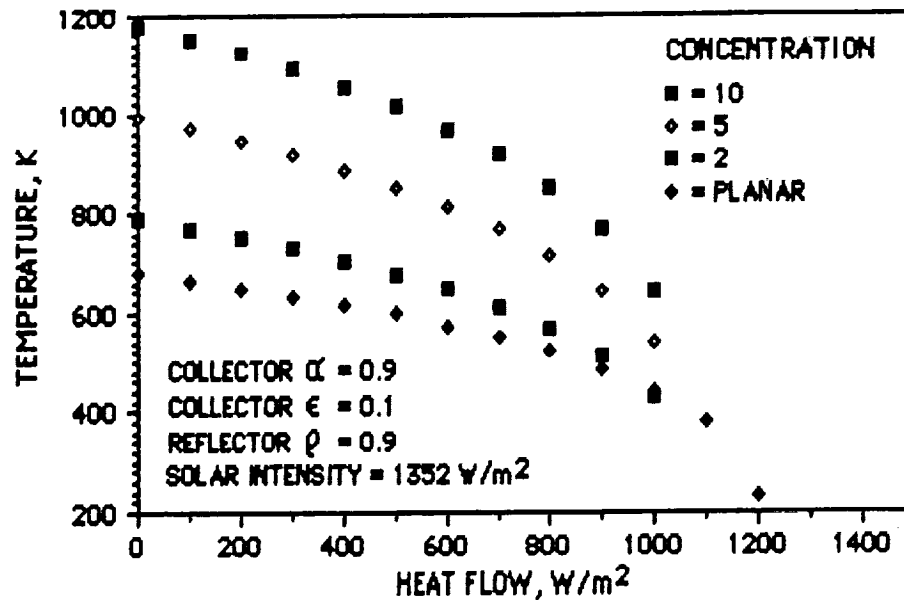


Figure 3-1. Solar thermal heat sources in Earth or Moon orbits.

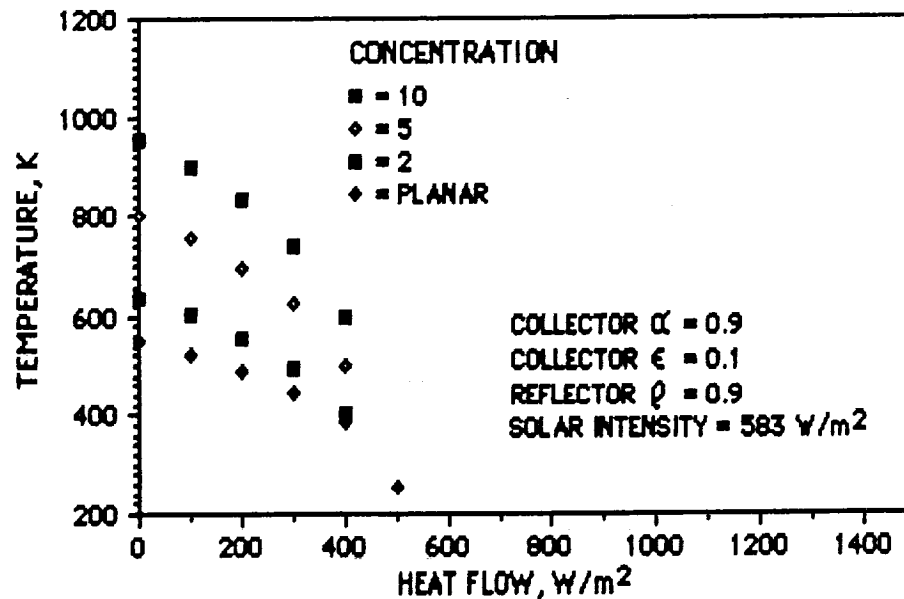


Figure 3-2. Solar thermal heat sources in Mars orbit.

insolation respectively). Four cases are shown in each plot; concentration factors 2, 5 and 10, and the planar case (concentration factor =1). All collectors are assumed to have absorptivities of 0.9 and emissivities of 0.1. The reflectors for the concentrators are assumed to have a reflectivity of 0.9. The prospects for solar thermal collectors are fairly good in Earth or Moon orbits. Moderate temperature hydride applications (ca. 400 K) could draw about 1 kW/m² from a planar array. At higher temperatures (e.g., 700 K), concentrating collectors with concentration factors of about 10 would provide nearly 1 kW/m² in Earth or Moon orbits.

In Mars orbit, the opportunity to use solar thermal energy is considerably diminished by the reduced solar intensity. Figure 3-2 indicates that only 400 W/m^2 could be collected at 400 K by a planar array. A 10x concentrating array at 700 K could only provide about 350 W/m^2 .

Bases at most lunar surface sites must operate in darkness for two weeks at a time. Mars' surface is also affected by diurnal variations and the reduced intensity noted in Figure 3-2 is further limited by its atmosphere. Clouds and frequent dust storms, and seasonal variations contribute to the difficulty of implementing solar electric or thermal power on Mars. The need for large deployable structures complicates the use of solar power aboard spacecraft which experience large accelerations. Nuclear power is a prime alternative in each of these circumstances.

It has been decided that the SP-100 nuclear power system will be a radioisotope thermoelectric generator (RTG) instead of the Sterling, Brayton or thermionic alternatives (Harless, 1987). The use of nuclear power in near-future spacecraft and planetary bases will likely be similar to the SP-100. The more distant future may hold new alternative power conversion methods (e.g., Bankston and Shirkbacheh, 1986) as well, but in every foreseeable case there is an opportunity for acquiring waste heat at relatively high temperature for powering metal hydride devices. Figure 3-3 indicates that the mass of an SP100 RTG is minimized, in trade-offs between reactor and shielding size vs. radiator area, at a temperature of about 930 K (657°C). This is very high temperature waste heat compared to what has been used in most terrestrial hydride applications. The higher temperatures will necessitate some changes in the hydride materials, their containers and the heat transfer fluids that carry heat from the nuclear power system to the hydride containers. The SP100 RTG converts about 6% of its 1.67 MW heat output to electricity (Ewell, 1981). That leaves up to 1.57 MW available as thermal power that might be used to operate metal hydride cycles.

Fuel cells may also be useful as heat sources for hydride thermal cycles. Regenerative fuel cells could supplement solar power systems on the dark sides of orbits, and chemical reactants could power surface vehicles via fuel cells. The thermal power rejected from a fuel cell is commensurate with its electric power (i.e., $\approx 50\%$ efficient). Fuel cell waste heat rejection temperatures are typically $<100^\circ\text{C}$.

The key to effective use of waste heat to power metal hydride devices lies in understanding that the heat must eventually be rejected at a lower temperature. This necessitates larger radiator area with consequential costs



SP-100 THERMAL OPTIMIZATION

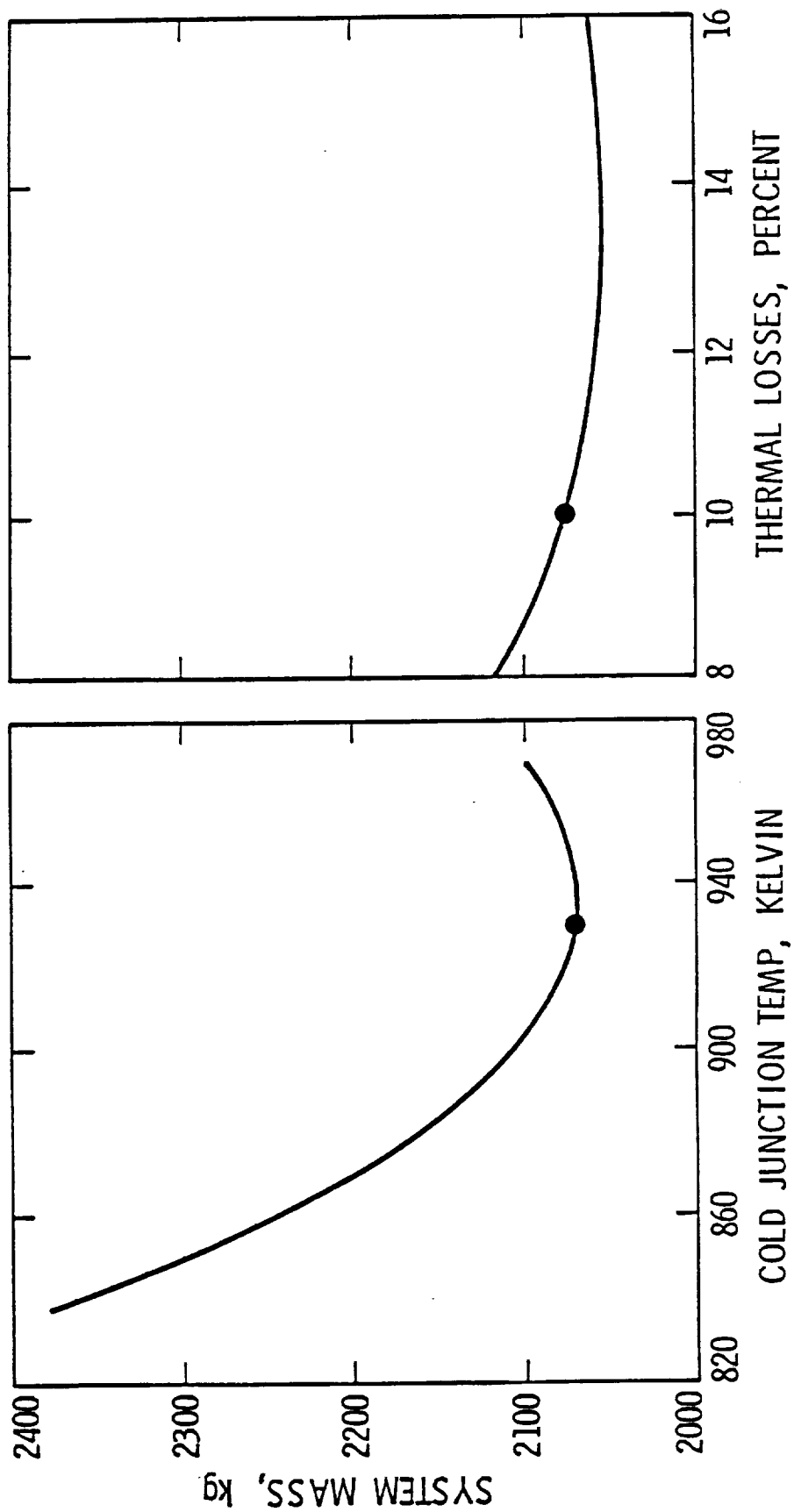


Figure 3-3. Thermal optimization of the SP-100 (copied from Ewell, 1981).

in terms of mass and volume. Hydride devices in space can pay for their passage in several ways. One way is by conserving electric power so that the mass credit associated with reducing the load on the power system compensates for the mass of the hydride device, including the extra radiator area. The SP-100 RTG has a projected mass of about 2800 kg (Giudici, 1986) and a capacity of 100 kW, so the power-mass "penalty" added to the mass of an electrically powered subsystem is 28 kg per kW, plus additional mass for power conditioning, distribution, and thermal management.

A second way to reduce electric power system mass with hydride thermal subsystems is to reduce the need for stored electricity. This accrues a mass credit for conserving electricity, and an additional mass credit for reducing electrical storage requirements. Storage requirements contribute significantly to the 159 kg/kW power-mass penalty of the solar powered Space Station's reference configuration (NASA, 1984).

3.2 ENVIRONMENTAL CONDITIONS

Temperature and its variability in each particular space mission determine the types and sizes of thermal system components that will be needed. On Mars, a food storage freezer might be simply an uninsulated box exposed to the environment. On the Moon that same box would alternately become a freezer and an oven in a two week cycle.

SPACECRAFT ENVIRONMENTS

Assembly and checkout of lunar and planetary spacecraft prior to departure and post return operations may take place in LEO or at transportation depots at Earth-Moon or Sun-Earth libration points. An orbit (ca. 90 min.) coordinated with the Space Station would facilitate interaction with the Space Transportation System. If LEO is the alternative selected, the thermal control system must be capable of coping with orbital light/dark cycles and Earth's albedo and IR emission. LEO will be the warmest spacecraft thermal environment for spacecraft bound for the Moon or Mars. Table 3-1 compares the solar, reflected, and IR fluxes in low orbits around Earth, the Moon and Mars. IR emission varies with surface temperature, emissivity, and atmospheric composition (CO_2 , H_2O) and conditions (clouds, dust, etc.) on Earth and Mars. The solar intensities, albedos, temperatures and emissivities used to construct Table 3-1 were obtained from the literature (Martin Marietta, 1970; Kopal, 1971; Alter and Clemminshaw) with judgement by the authors where ranges of values were published or where there was a disagreement in published values. The values used are listed in the "Notes" column at the right of Table 3-1.

Table 3-1. Nominal solar, reflected, and infrared fluxes in low orbit around Earth, the Moon and Mars. All values are in Watts per square meter (BTU/hr per ft² in parentheses).

	Solar	Reflected	IR	Notes
Earth	1352 (429)	406 (129)	236 (75)	Data from Martin Marrieta, T-70-48874-011
Moon	1352 (429)	95 (30)	200 (63)	Calc. @ A=0.07 T _s =253K, ε=0.9
Mars	583 (185)	87 (28)	38 (12)	Calc. @ A=0.15 T _s =165K, ε=0.9

Table 3-1 shows that all radiant fluxes are significantly reduced in low lunar and Mars orbits. It is also significant that Mars orbits may not be "low", in the sense of nearly hemispherical exposure to the planet. Higher orbits will be colder yet. During the greatest portion of a Mars mission, the spacecraft will be in transit, too far from the Earth or Mars for either of them to influence thermal system performance. The Sun is the only source of radiant energy that must be considered during Earth-Mars space travel. As indicated in Table 3-1, nominal solar intensity ranges from 1352 W/m² (429 Btu/hr-ft²) near the Earth, to 583 W/m² (185 Btu/hr-ft²) as the spacecraft approaches Mars.

It would not be efficient to optimize hydride subsystems or other thermal control system components for LEO and then carry the excess mass on missions to cooler orbits. The advantages of deployable, steerable radiators in cold environments may not justify their added mass and complexity. Body-mounted radiators or single-axis radiators mounted to structural booms could serve nearly as well, once the spacecraft departs LEO. If hydride subsystems were compromised to operate with a restricted radiator capacity in LEO, their masses would increase (lower ΔT-->longer cycle time-->greater mass for a given heat flow). An auxiliary system could serve the temporary thermal control demands, while the spacecraft is in LEO. The auxiliary thermal control system could be left behind when the spacecraft departs LEO. This potential hydride application will be examined in Section 4 of this report.

LEO is not the worst case orbit for thermal storage. The orbital periods of some spacecraft may be much longer than LEO. High Mars orbits of 24 hours or more are under consideration to minimize round-trip propellant requirements (Babb and Stump 1985). The dark side of a Mars orbit might be 4 hours or more.

THE LUNAR ENVIRONMENT

The nominal solar intensity at the Moon is the same as LEO, averaging 1352 W/m^2 . The 29 day lunar cycle is the longest diurnal cycle in the Earth-Mars system. During the 2-week lunar day, surface temperatures rise to 405 K (270°F), and the 2-week night drops temperatures to 105 K (B. French, 1977). Polar sites may avoid most of the diurnal variation, and temperatures are thought to be less than 100 K in the shade (Burke, 1984). Thermal control system types and capacities will be strongly influenced by site selection. Polar sites could be powered by solar energy throughout the lunar cycle whereas nuclear power seems the only realistic alternative at other locations. The environment is relatively constant at the poles so thermal storage requirements are not unreasonably large.

Radiators on the Moon are likely to be ultralight panels lain flat on the surface to minimize structural mass. During peak daytime periods these radiators will receive the full radiant input of the sun, and the albedo and IR inputs from nearby tall surface objects (e.g., mountains, structures). On the Moon it is apparent that the performance of present state-of-the-art radiators in worst case insolation will fall off rapidly at temperatures below about 300 K at all but polar sites. This points to a need for some type of heat pumping or very large thermal storage capacity to manage lower temperature heat loads, including metabolic cooling and refrigeration, during peak daylight periods.

Passive temperature stabilization in surface structures on the Moon is a challenging task that may only become feasible in growth phases of lunar base development if thermal storage materials (e.g., hydrides) are manufactured on the Moon. Landers, rovers and above ground structures could be well insulated to minimize inward heat leak during the lunar day. The thermal control system would remove the small inward heat leak plus interior heat loads by heat pumping. Nuclear power systems can provide adequate heating during the lunar night. For thermal stability, as well as for shielding against solar and cosmic radiation, living and working structures will probably be located underground. Loose soil (regolith) in a hard vacuum is good insulation (B. French, 1977). A few meters under the surface, the temperature is nearly constant at 253 K (-5°F). It may be possible to locate the lunar base in the nearly constant temperature environment of volcanic lava tubes (Hörz, 1984).

THE MARTIAN ENVIRONMENT

The use of radiators on the surface of Mars is a difficult problem to analyze because Mars' sky is so variable. The "brightness temperature" of an object, T_b , is the temperature at which a black body emits the same spectral radiance as the object. T_b in the Martian sky reaches its minimum value of about 130 K near the south pole during the southern winter. Maximum southern summer T_b values of about 230 K occur at moderate latitudes. During the southern summer (northern winter), global dust storms contribute to the IR opacity of the atmosphere, raising temperatures all over the planet.

In addition to radiant cooling, radiators and other heat exchangers on Mars will shed heat to the thin atmosphere by convective cooling. Library computer searches* did not turn up any published information on the heat transfer properties of the Martian atmosphere. There is, however, enough published information about the pressure, temperature, and composition of Mars' atmosphere (Kliore, ed., 1982) to allow these properties to be calculated.

Neglecting trace amounts of minor constituents, the Martian atmosphere has the composition described in Table 3-II.

Table 3-II. Major constituents of the Martian atmosphere (Seiff, 1982).

Component	Mole Fraction	Molecular/Atomic Weight
CO ₂	0.9555	44.009
N ₂	0.0270	28.018
Ar	0.0160	39.961
O ₂	0.0015	31.998

The molecular and atomic weights of N₂ and Ar are slightly different from the corresponding terrestrial values because of the slightly different isotopic ratios for these two elements on Mars (Owen, 1982). The average molecular weight for this model Martian atmosphere turns out to be 43.494.

* Both the Colorado Association of Research Libraries and the Lunar and Planetary Institute in Houston ran several obvious key words to no avail.

Transport properties of the Martian atmosphere were calculated by determining values of constant pressure heat capacity C_p , viscosity μ , and thermal conductivity k , for each of the four separate compounds, and then combining these last two by the mixing rules of Wilke (Edwards et al., 1976). Densities were computed from the ideal gas law, allowing the Prandtl numbers to be completely determined, and supplying the fluid-dependent properties for the complete determinations of the Reynolds, Grashof and Nusselt numbers in each particular heat transfer geometry.

Heat capacities were determined as functions of temperature for the individual molecules by the rigid rotor harmonic oscillator approximation (Hill, 1960), and then converted back to molar values and summed over mole fractions. Both the viscosity and thermal conductivity were determined for the Lennard-Jones 6-12 potential (Hirschfelder et al., 1964) involving the omega collision integrals (ibid.) as functions of temperature.

The calculated Martian planetary surface atmospheric transport properties for the four constant-composition model atmospheres given in Seiff (1982) are presented in Table 3-III.

TABLE 3-III. Martian planetary surface atmospheric transport properties computed from Lennard-Jones 6-12 potential model.

Atmosphere Description (REF)	T (K)	P (mbar)	ρ (kg/m ³)	C_p (J/kg·K)	μ (Pa·s)	k (W/m·K)	Pr = $C_p \mu / k$
Daily & northern summer-seasonal mean midlatitude	214	6.36	1.58 E-2	7.52 E+2	1.10 E-5	1.09 E-2	0.758
Daily & southern summer-seasonal mean midlatitude	214	7.3	1.81 E-2	7.52 E+2	1.10 E-5	1.09 E-2	0.758
Cool, low pressure midlatitude daily mean	204	5.9	1.53 E-2	7.42 E+2	1.05 E-5	1.03 E-2	0.754
Warm, high pressure midlatitude daily mean	224	7.8	1.85 E-2	7.63 E+2	1.15 E-5	1.15 E-2	0.760

With the transport properties collected in Table 3-III, values of the surface convective heat transfer coefficient h ($\text{W/m}^2\cdot\text{K}$) were calculated (Eckert, 1974) for configurations that would be potentially useful for cooling hydrides as well as other thermal system components on Mars. Table 3-IV shows the results for both Martian and Earth surface conditions. The right hand column of Table 3-IV indicates the relative performance of each case as a ratio $h_{\text{Earth}}/h_{\text{Mars}}$.

The last two lines of Table 3-IV are for the values of the height H of the rectangular duct of width 1.0 m that make the Reynolds number equal to 2800, the transition limit between laminar and turbulent flow between parallel plates (Edwards et al., 1976). The surface atmospheric velocity of 10 m/s (22.4 mph) is a good average for the widespread Martian winds modeled for midlatitudes (Leovy, 1982), although it is too high for average winds on the Earth's surface.

Of the configurations considered below, that of cylinders with forced crossflow convection seems to have the most promise for use on the Martian surface.

The combined effects of radiation and convection in the Martian atmosphere will improve the performance of heat dissipating panels, such as those in the portable life support systems (PLSS) of EMUs. Nonventing EMUs for the Space Station will have approximately 1 m^2 of radiator surface at a temperature of up to 319 K (115°F). If the same radiator area and surface temperature were available on a Mars EMU, convection would provide additional heat rejection capacity. Modeling the backpack of the EMU as a vertical panel, Table 3-II indicates that 1 m^2 of vertical panel area will shed between 0.20 W/K (no wind) and 0.42 W/K (10 m/s wind), depending on wind conditions. A typical temperature difference might be $319 \text{ K} - 214 \text{ K} = 105 \text{ K}$. The improvement in heat flow would be between 21 W and 44 W depending on wind conditions.

The availability of CO_2 and H_2O from the Martian environment appears to be a prime alternative for refrigeration, heat pumping, and thermal storage applications. It is possible that a Mars base would be located near one of the poles to gain access to the "dirty water ice" caps. In that case, the solid CO_2 - H_2O mixture, gathered from the surface, could serve as a refrigerant. Cold plates in reservoirs on vehicles, EMUs, etc. could provide an effective and ultra-simple cooling method in circumstances where direct radiation plus convective cooling are inadequate. The sublimation and boiling properties of the solid and liquid phases of CO_2 and H_2O were included in Table 1-1 to contrast them with the alternatives.

TABLE 3-IV. Values of surface convective heat transfer coefficients, h ($W/m^2 \cdot K$) for selected flow and geometry. All cases were evaluated for both the planetary surface Martian Nominal Model Daily & Southern Seasonal Mean Midlatitude Atmosphere (214 K and 7.3 millibars (Seiff, 1982)) and for nominal Earth surface conditions (288.7 K and 1.0 atm). Laminar or turbulent flow are indicated as (L) or (T).

Configuration	h_{Mars} (SI)	h_{Earth} (SI)	h_{Earth}/h_{Mars}
Vertical flat plate Forced convection @ 10 m/s and 1.0 m from leading edge	0.42 (L)	28.5 (T)	68
Vertical flat plate Natural convection @ 1.0 m from leading edge	0.20 (L)	2.84 (T)	14
5/8" OD cylinders with Forced convection Crossflow @ 10 m/s	5.6 (L)	80.7 (L)	14
Rectangular duct with 1.0 m width, variable height H , and 10 m/s forced convection:			
$H = 0.1$ m	0.76 (T)	34.3 (T)	45
$H = 1.0$ m	0.54 (T)	24.4 (T)	45
$H = 2.03 \times 10^{-3}$ m (transitional H on Earth)	---	146(T), 96.2(L)	
$H = 9.3 \times 10^{-2}$ m (transitional H on Mars)	0.77 (T), 1.02 (L)	---	
(Comparison made at transitional H)			190(T), 94(L)

At mid-latitudes on Mars, CO₂ could be liquefied from the atmosphere by compression or solidified by refrigeration. The CO₂ pressure-enthalpy diagram (Canjar et al., 1966) is shown in Figure 3-4. In the atmospheric pressure range of Mars (ca. 8×10^{-3} Earth atmospheres), CO₂ will solidify at about 150 K (-190°F). A refrigerator cold plate below this temperature would extract crystals of solid CO₂ from the atmosphere that could be used for a variety of thermal system applications. At pressures above the triple point (5.1 Earth atmospheres) the liquid phase could be formed in condensers and used as a working fluid in heat pumps or refrigeration cycles at temperatures up to the critical temperature of 304 K (88°F). An idealized -30°C (-22°F) refrigeration cycle, A-B-C-D, with a 3.4:1 vapor compressor and heat rejection to a 15°C (59°F) radiator, is drawn in Figure 3-4 as an example of how CO₂ might be used in thermal control applications.

PHOBOS' AND DEIMOS' ENVIRONMENTS

Mars' satellites, Phobos and Deimos, may be carbonaceous chondrites that contain precious volatile elements (Duke, 1986). If hydrated minerals are exploited for propellants, etc., a portion of the water produced could be used in Shuttle-type sublimation coolers. The gravimetric and volumetric heats of vaporization of water in its liquid and solid phases were listed in Table 1-1.

The solar intensity, I_s , in Mars orbit at the surfaces of Phobos and Deimos ranges between 487 and 709 W/m² compared to the Moon and Earth range of 1309 to 1399 W/m² (Giudici, 1986). The worst case environment for radiators on a martian moon occurs at noon at an equatorial site during the closest approach of Mars' elliptical orbit to the sun. Assuming a present state-of-the-art radiator surface (Ag-backed TFE, $\alpha = 0.10$, $\epsilon = 0.75$), placed flat on the surface, the radiant heat flux is calculated as follows:

$$\begin{aligned}\dot{Q} &= \alpha I_s - \epsilon \epsilon_r T_r^4 \\ &= 0.10 (709 \text{ W/m}^2) - (5.6697 \times 10^{-8} \text{ W/m}^2 \text{ K}^{-4})(0.75) T_r^4\end{aligned}$$

The outward flux (negative), as a function of temperature, is plotted in the 200 - 400 K range in Figure 3-5. It is apparent that low temperature heat rejection in a worst case environment at Phobos or Deimos will require a significant radiator area. For example, metabolic heat rejection (277 K) for a crew of 3 would require about 5 m² (54 ft²) of radiator area. One kW of refrigeration (250 K) corresponds to 13 m² (140 ft²) of radiator area under these conditions.

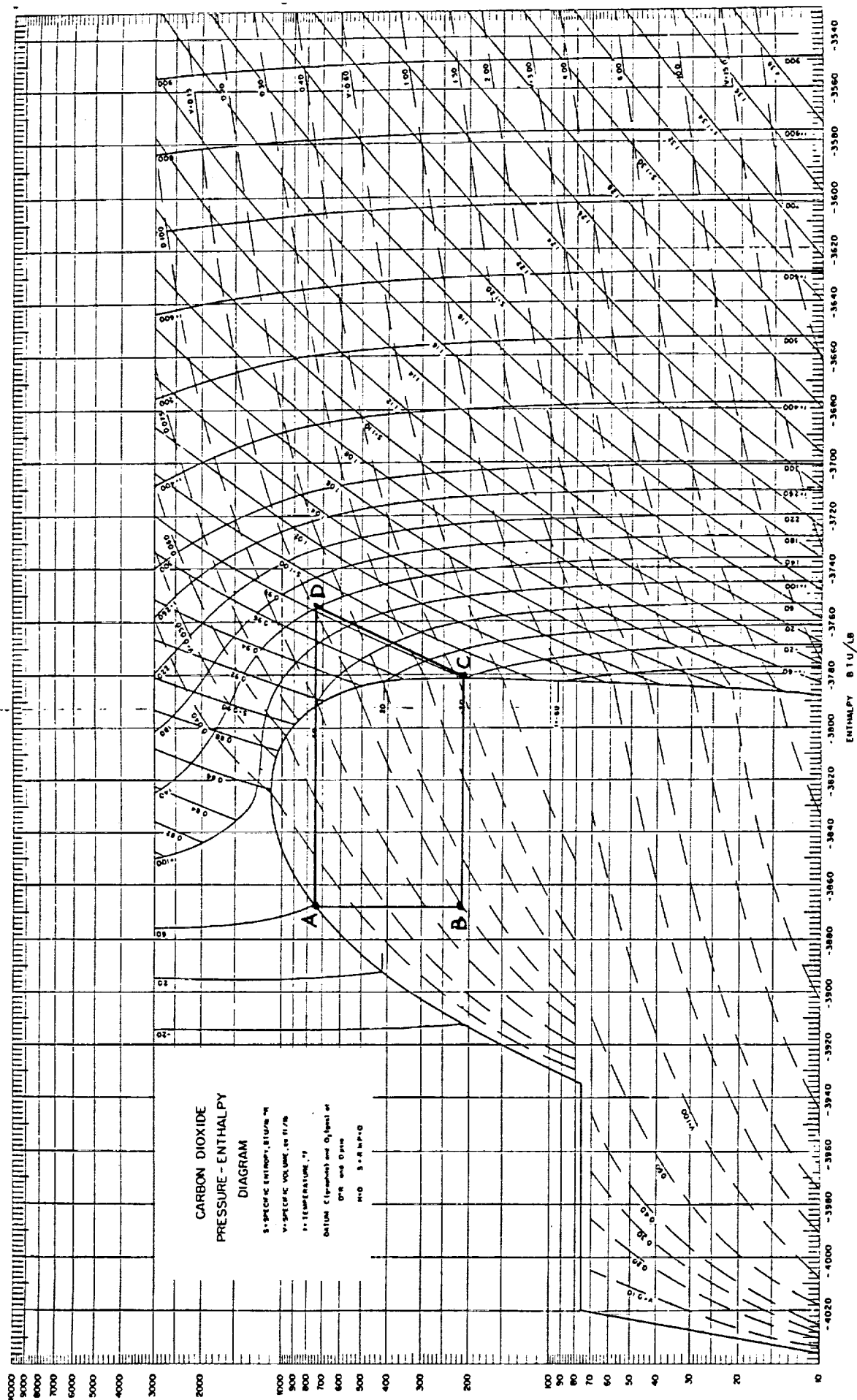


Figure 3-4. CO₂ pressure-enthalpy diagram with a typical refrigeration cycle, A-B-C-D, that might be useful at a Mars Base (diagram copied from Canjar et al., 1966).

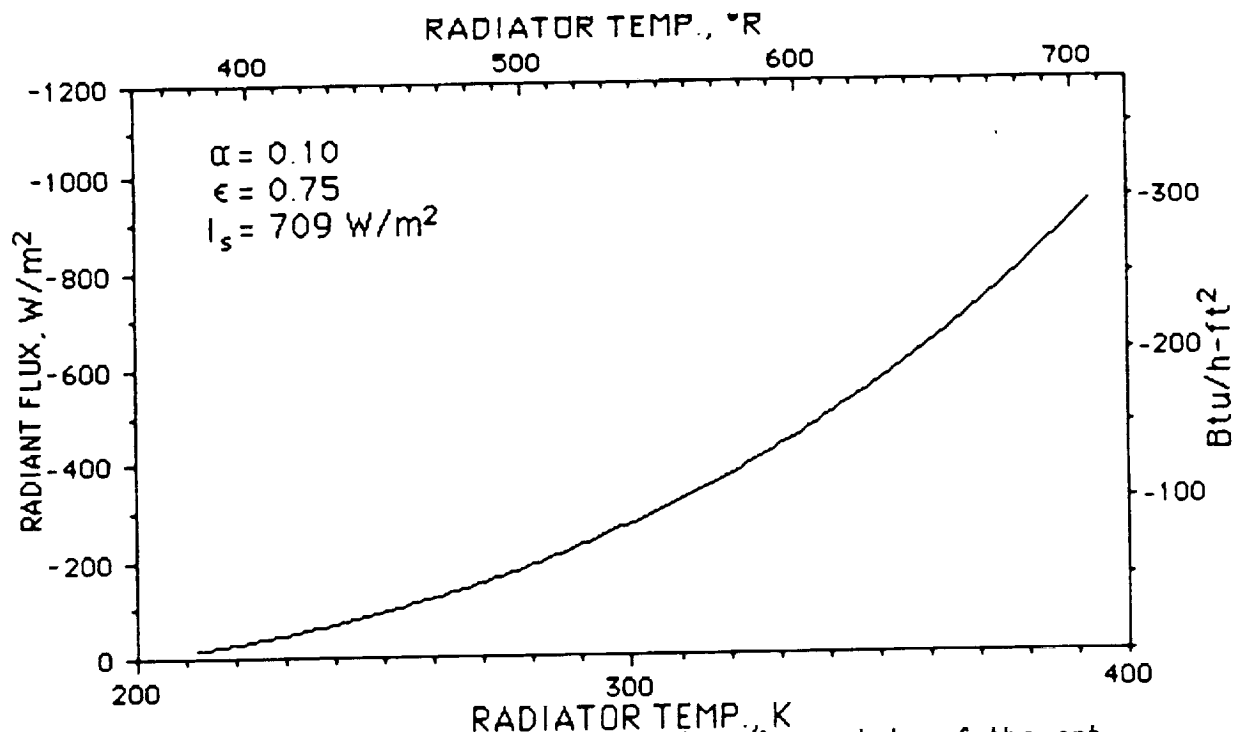


Figure 3-5. Radiant heat flux vs. temperature for a state-of-the-art radiator at the surfaces of Mars' moons. The worst case, noon at minimum distance to the Sun, is shown.

3.3 CONDUCTION OF HEAT INTO SUBSURFACE ROCK

The surfaces of Earth's Moon, Mars and its moons have immense heat capacities that could serve as sinks for thermal systems (Comer, 1986). Drilling equipment will be needed for a number of scientific and construction-related purposes at lunar and planetary bases. Blacic, Rowley and Cort (1986) describe several drilling techniques that may be used on Mars. The equipment shown in Figure 3-6 is intended to bore holes up to 100 m deep and 15 cm in diameter. For similar purposes, Rowley and Neudecker (1984) have discussed drilling equipment for use on the Moon. The drill holes might serve a number of useful purposes beyond that for which they were originally bored. There may be a permafrost layer of water ice below the surface of Mars that could be melted and withdrawn from the hole while dissipating waste heat from power or thermal systems (Duke, 1986).

Since the mass of the drilling equipment can be written off against its primary purposes, drill holes might be a very efficient means of dissipating heat in terms of mass and volume launched from LEO. The heat exchanger to be

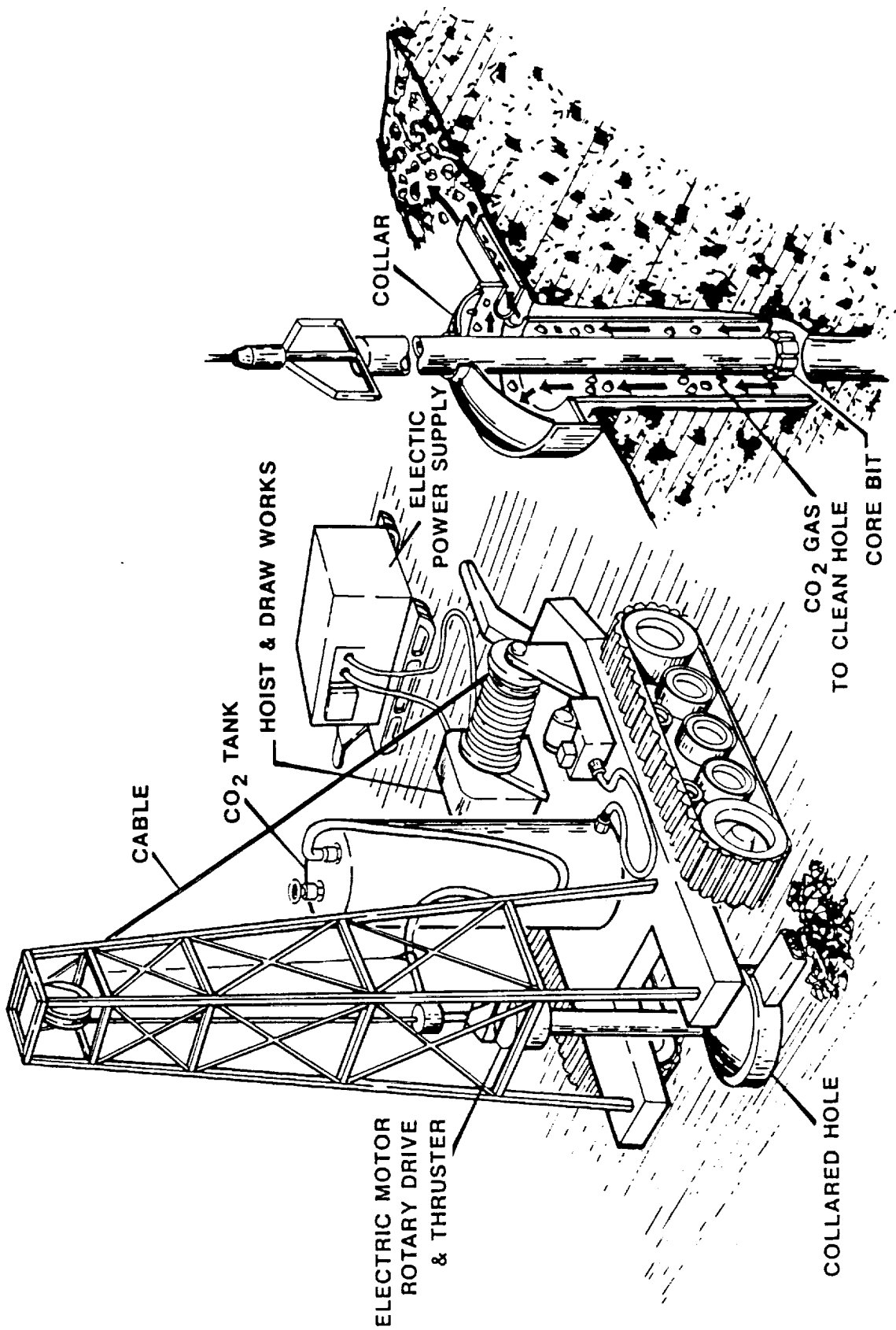


Figure 3-6. General Concept for a Mars Drilling Rig (copied from Blacic, Rowley and Cort, 1986).

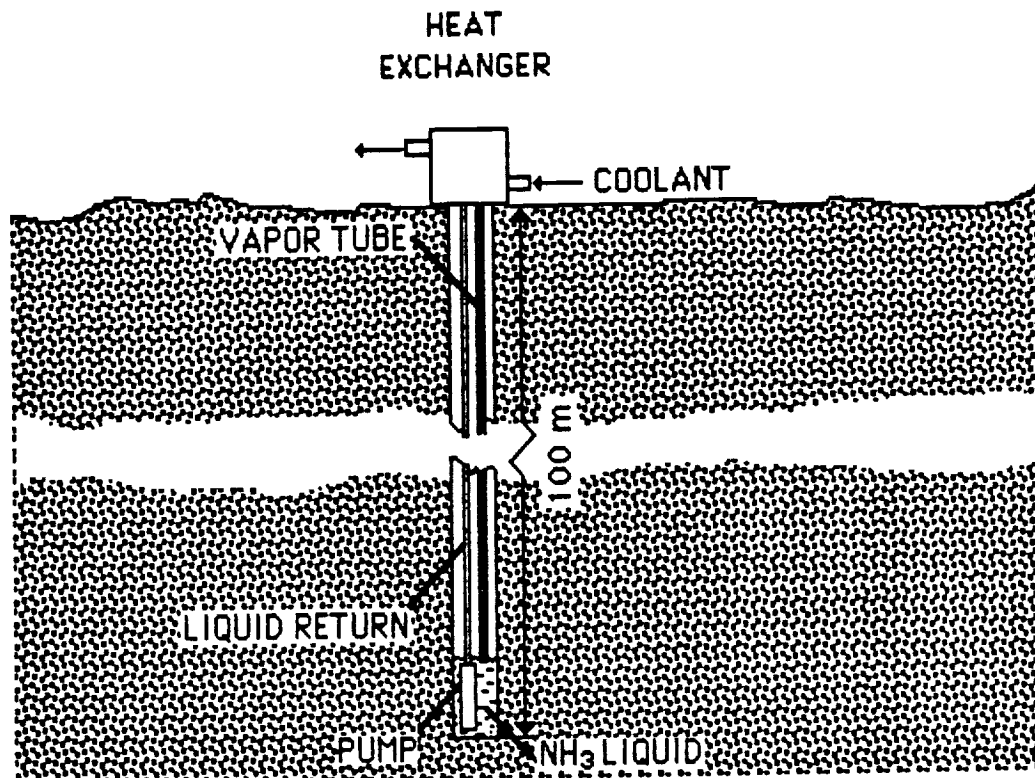


Figure 3-7. Gravity flow pumped ammonia heat pipe carries heat from the heat exchanger to subsurface rock.

inserted in the hole would be the main item transported from Earth. If its mass and volume were significantly less than the alternatives, such as radiators or atmospheric heat exchangers (Mars only), the concept could have merit. Among other advantages, the subsurface heat exchanger is protected from meteorites.

Figure 3-7 shows a series of heat pipe segments linked together and installed in a drill hole in a manner similar to drill rod assembly. This could be accomplished by the drill rig with no extra tooling. After installation, a high conductivity epoxy or a cement formed from local materials might be poured around the heat pipe and any other down hole items such as a water extraction pump, tubing and instrumentation.

In *Boundary Value Problems of Heat Conduction*, M. Necati Ozisik solves the problem of conducting a steady heat flux from a cylindrical hole into a surrounding medium utilizing the heat conduction equation in cylindrical coordinates. Assuming that the initial temperature of the medium is T_0 at time zero, a temperature change $\Delta T = T(r,t) - T_0$ will be transmitted into the medium adjacent to the hole. Assuming temperature independent thermal properties, the solution of the problem is not affected by the particular value of T_0 . It simplifies the notation to assume that $T_0 = 0$ so that $\Delta T = T(r,t)$. A temperature distribution of the form $T = (a_1 + a_2 r + a_3 r^2) \ln r$ is assumed which closely approximates a more lengthy exact solution to this problem (Ozisik, 1968).

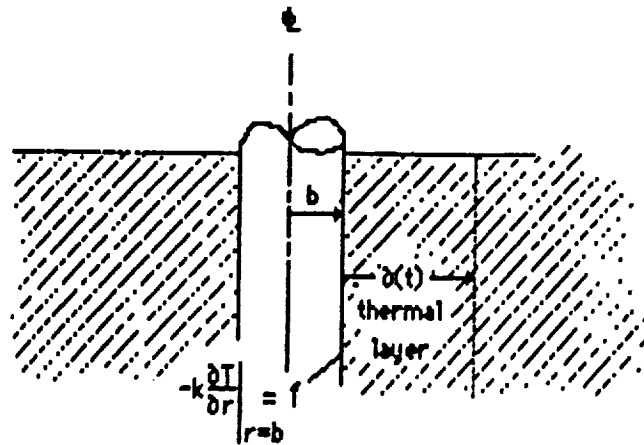


Figure 3-8. A constant heat flux, f is conducted from a cylindrical hole to a growing "thermal layer" $\delta(t)$ thick in the surrounding medium.

The unknown coefficients a_1 , a_2 , a_3 are determined from three conditions: 1) flux at $r=b$ is constant; 2) flux at the boundary of the thermal layer is zero; and 3) temperature outside the thermal layer = 0°C . Conditions 1), 2), and 3) are shown respectively below:

$$-k \left. \frac{\partial T}{\partial r} \right|_{r=b} = f \quad -k \left. \frac{\partial T}{\partial r} \right|_{b+\delta(t)} = 0 \quad T \Big|_{b+\delta(t)} = 0^\circ\text{C}$$

For any time, t the thermal layer thickness, $\delta(t)$ is found by utilizing the following equation in conjunction with an integral halving technique.

$$\frac{\alpha t}{b^2} = - \left[\frac{(72\eta^2 - 96\eta + 36) \ln \eta - 13\eta^4 + 36\eta^2 - 32\eta + 9}{144(\eta - 1)(2 \ln \eta + \eta - 1)} \right]$$

where

$$\eta = 1 + \delta/b$$

The temperature at the surface of the hole may then be calculated since temperature is a function of the thermal layer thickness (δ). It turns out to be:

$$T \Big|_{r=b} = \frac{fb}{k} \cdot \frac{\delta}{b} \cdot \frac{\ln(1 + (\delta/b))}{2 \ln(1 + (\delta/b)) + \delta/b}$$

Using these relationships, a computer program has been written that finds time and hole temperature when values are input for a thermal layer thickness and steady state heat flux applied to the heat exchanger surface. Other necessary input values are the properties of the thermal layer. Specifically, these properties are thermal conductivity, k ; specific heat, C_p ; and density, ρ .

Basalt is typical of the rock under a thin layer of regolith in the lunar maria. There may also be thinly covered basalt layers in the volcanic regions of Mars. The following basalt properties were used in order to simulate a lunar/martian subsurface heat sink.

$$\rho_{\text{basalt}} = 2790 \text{ kg/m}^3$$

$$k_{\text{basalt}} = 2.17 \text{ W/m K}$$

$$C_{p_{\text{basalt}}} = 837.2 \text{ J/kg K}$$

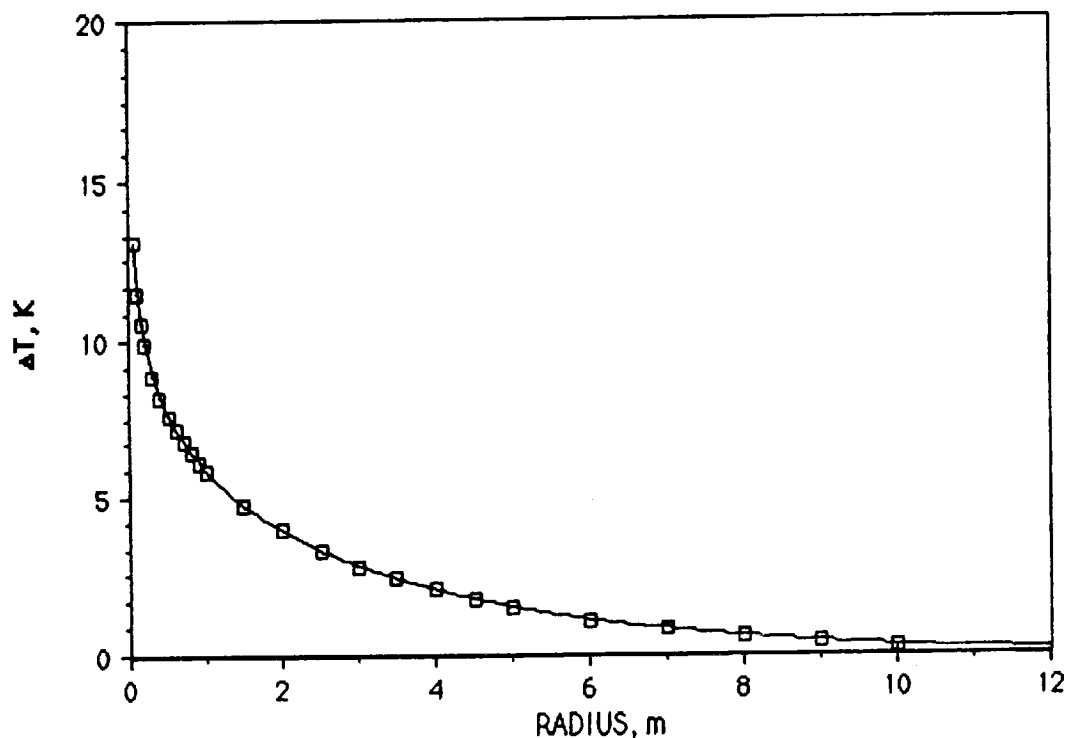


Figure 3-9. Variation of rock temperature with radius from the center of a 10 cm diameter hole after 1 Earth-year of use as a heat sink for a 100 W/m^2 thermal load.

Figure 3-9 is a profile of temperature versus radius within the thermal layer in a basalt heat sink after a working period of one year at a heat flux of 100 W/m^2 . The maximum ΔT at the heat exchanging surface is only about 13 K after a year of service. The thermal layer extends to a radius of 18.25 meters in this period, but the increase in temperature is less than 2 K only 4 meters from the surface of the hole.

Figure 3-10 shows how the temperature at the hole radius, $b = 5 \text{ cm}$ changes with time at different heat fluxes. The subsurface rock of the Moon, Mars, Phobos and Deimos are all cold enough to provide adequate metabolic and equipment cooling at reasonable heat fluxes for many years. For example, suppose that an equipment cooling loop dissipates a steady heat flow of 10 kW into a 5 cm radius x 100 m deep hole in the floor of a lunar cave for a period of 1 year. The hole would have an inside surface area of 31.4 m^2 so the heat flux would be 0.318 kW/m^2 . Figure 3-10 shows data for 0.1 kW and 1.0 kW, bracketing the heat load of this example, and indicates a temperature rise of about 30 K at the end of 1 year. The original temperature of the lunar rock would be about 253 K, so the inside of the hole would have reached 283 K--still cool enough for an equipment loop (ca. 293 K or 20°C). The curves are nearly flat as they pass the 1 year mark so several more years (perhaps indefinite) service can be expected from the sink.

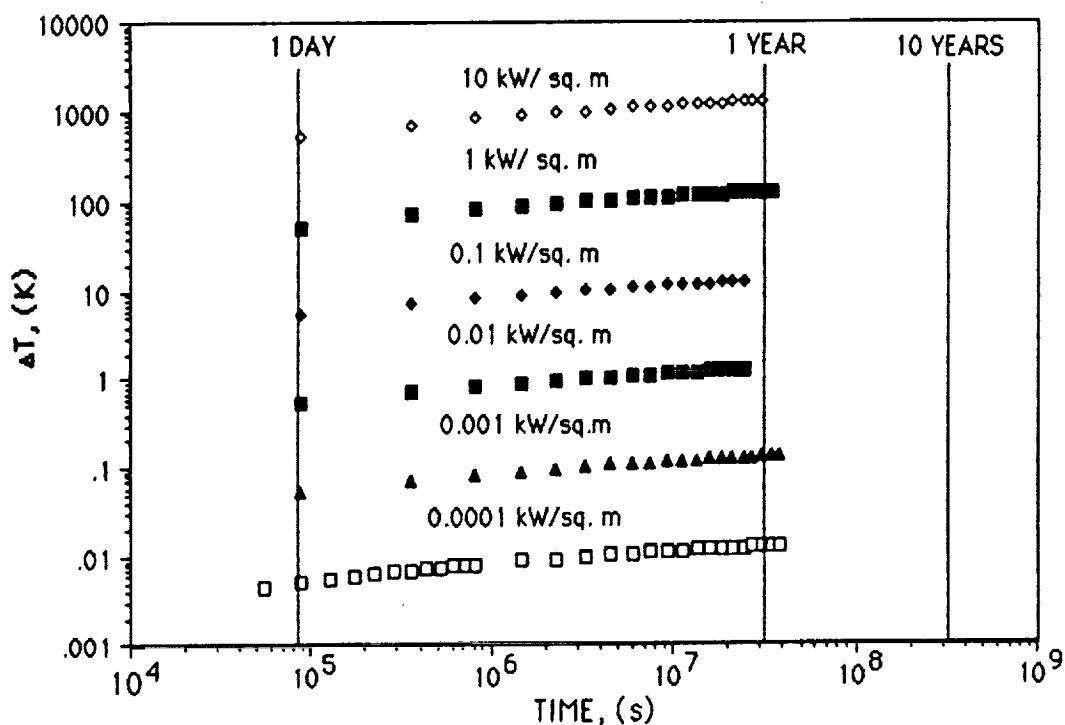


Figure 3-10. Temperature rise vs. time in log-log coordinates for several ranges of heat flux from a 5 cm radius hole in basalt.

As a check on Ozisik's model and HCI's programming, a numerical integration of the sensible heat content of the rock from $r=b$ to $r=\infty$ (1 year) was made and compared to the cumulative heat dissipated at a steady rate of 100 W/m^2 for 1 year. The two calculations agreed within 1% that 10^9 Joules would be absorbed by the basalt for each meter of hole depth at the end of 1 year.

4.0 HYDRIDE APPLICATIONS IN FUTURE SPACE THERMAL SYSTEMS

The preceding sections of this report have outlined the use of metal hydrides in thermal systems and the environmental factors that will determine the operating conditions of thermal systems in future space activities. This section will combine that information to identify concepts for utilizing hydrides to enhance thermal system performance in future space missions.

Most of the cooling requirements in space or at lunar and planetary bases could be served by direct radiation. However, the radiator area needed for each unit of thermal power rejection grows as the temperature of the cooling load decreases. The radiator area requirement for a given mission will decrease if heat pumping is used to increase the rejection temperature and if thermal storage is available to buffer the peak heat loads. As explained in Section 2 of this report, hydride thermal subsystems can perform as heat pumps and as thermal storage devices (see Figs. 2-4 and 2-5).

Viable heat pumping and thermal storage alternatives must provide overall system improvements in terms of mass, volume, power consumption, drag and many intangible factors, compared to a simple (but large) radiator. Hydride refrigerators, heat pumps and thermal storage devices are thermally powered. They compete well with electrical cooling alternatives when a suitable heat source and sink can be provided without unreasonable system compromises. Reduction of radiator area via electrically powered (i.e., vapor compression or thermoelectric) heat pumping suffers from the *power-mass penalty* (e.g., 159 kg/kW on the Space Station) amplified by certain system inefficiencies (Sadunas and Lehtinen, 1985). Hydride thermal subsystems only require electric power for liquid circulation, so a large mass *credit* applies relative to electric alternatives.

For some applications, the most important advantage of hydride thermal subsystems is their compactness. Table 1-1 compared hydrides with other thermal storage materials on the bases of gravimetric and volumetric energy densities. Hydrides are the most compact non-venting alternative. This feature of metal hydrides is particularly advantageous in applications where mobility is critical. A prime example is a metal hydride heat pump for the regenerable nonventing thermal system of advanced extravehicular mobility units (EMU's) for the Space Station (Lynch and Riter, 1987). The same

advantages will pertain to advanced EMU's for future missions, and to other systems, such as rovers, where mobility will be hampered by large radiators.

In advanced stages of future space activities, raw materials may be mined and processed at the Moon, Mars, Phobos and Deimos. Hydrides are one of the few thermal storage alternatives that could be produced by refining known lunar and planetary Martian resources. Ilmenite (FeTiO_3) is a prospective feedstock for lunar oxygen production plants (Criswell, 1980; Williams and Mullins, 1983; Haskin, 1984; Gibson and Knudsen, 1984). Lunar thermal systems, based on FeTi-hydride, could be expanded indefinitely by further refinement of oxygen plant by-products. Other lunar and Martian minerals (e.g., olivines, pyroxenes) contain metals that would be useful for producing hydrides.

NASA's desire for *commonality* also encourages the use of hydride thermal subsystems since hydrogen is the working fluid. This presents opportunities for shared supplies between the thermal system and other hydrogen-related systems such as ECLS, fuel cells and cryogenic propulsion.

Internal studies at HCl also indicate that hydride thermal systems could synergistically provide shielding from solar and cosmic rays and nuclear radiation from power systems (see Section 4.5). Such dual use of hydrides could reduce the shielding mass that would otherwise be necessary on all extended missions outside of Earth's magnetosphere.

Each of the attributes of hydrides mentioned above will be illustrated in the following series of examples of hydride use in future thermal systems. The future space missions are not well defined at present, but the literature (Mendell, ed. 1985; Duke and Keaton, eds., 1986) provides a range of possible missions for which thermal system requirements may be projected.

4.1 LEO THERMAL ACCESSORY

Section 3.2 discussed the thermal environments that will be encountered by spacecraft in lunar and Martian missions. Table 3-1 indicates a significantly higher radiant flux in LEO than in subsequent space travel or low orbits around the Moon or Mars. In low orbits (e.g.; 360 km earth orbit, 100 km lunar orbit) the horizon subtends about 5 steradians of solid angle. At midday, the sum of the reflected solar and IR flux incident on a square meter of surface facing the earth will be about 510 W/m^2 (162 Btu/hr-ft^2). The same downward-facing surface at midday in low lunar orbit will intercept only 235 W/m^2 (75 Btu/hr-ft^2), and in low Mars orbit, only 99 W/m^2 (32 Btu/hr-ft^2). Sun-facing surfaces in Earth and Moon orbits will see about 1352 W/m^2 (429 Btu/hr-ft^2)

of solar flux, while Mars orbits will average only 583 W/m^2 (185 Btu/hr-ft^2). Earth orbit is clearly the warmest environment, and Mars orbit the coldest. Spacecraft surfaces and radiators will see 2.3 times as much insolation in LEO as in low Mars orbit and 5.2 times as much IR plus albedo. An additional factor is that Mars orbits may not be low (periods of 24 to 48 hours are under consideration) so IR and reflected solar radiation may be even less.

Clearly, a spacecraft thermal system designed for LEO will be much heavier than one of equal capacity for Moon or Mars orbits. For the same reasons that propulsion stages are left behind, it makes sense to detach excess thermal system capacity from a spacecraft before it leaves LEO. A detachable accessory thermal system, optimized for LEO, could provide extra radiator area, thermal storage, heat pump capacity, etc., without compromising the thermal system of a spacecraft bound for a cooler orbit. Figure 4-1 is a sketch of the concept showing an LEO accessory thermal system attached to a spacecraft prior to departure for Mars.

The excess thermal load could be rejected from accessory radiators. The size of the accessory radiators can be reduced by heat pumping. Hydrides could provide this heat pumping with very little increase in electric power demand because they are thermally powered. The only electric power needed is for circulation of fluids.

Section 3.1 summarized the opportunities to use solar thermal energy for powering metal hydride devices. In LEO, each m^2 of selective collector surface ($\alpha = 0.9$, $\epsilon = 0.1$) could provide about 1 kW of thermal power to a hydride heat pump. A flat plate collector on a sun-facing surface could provide the thermal power for the hydride heat pump, while the steerable radiators on the LEO thermal accessory dissipate the heat to space.

The process is illustrated in Figure 4-2. The upper half of the figure shows heat, applied by a solar thermal source, driving hydrogen out of hydride A and into hydride B. The heat liberated by hydride B as it absorbs hydrogen is dissipated by the radiator. This is the charging process that prepares the hydrides to deliver their cooling power (see Figure 2-5).

The lower half of Figure 4-2 shows the cooling process. Hydride B absorbs heat from the coolant loop as it desorbs hydrogen. The hydrogen flows into hydride A where it is absorbed exothermically and the heat of the reaction is shed to the radiator.

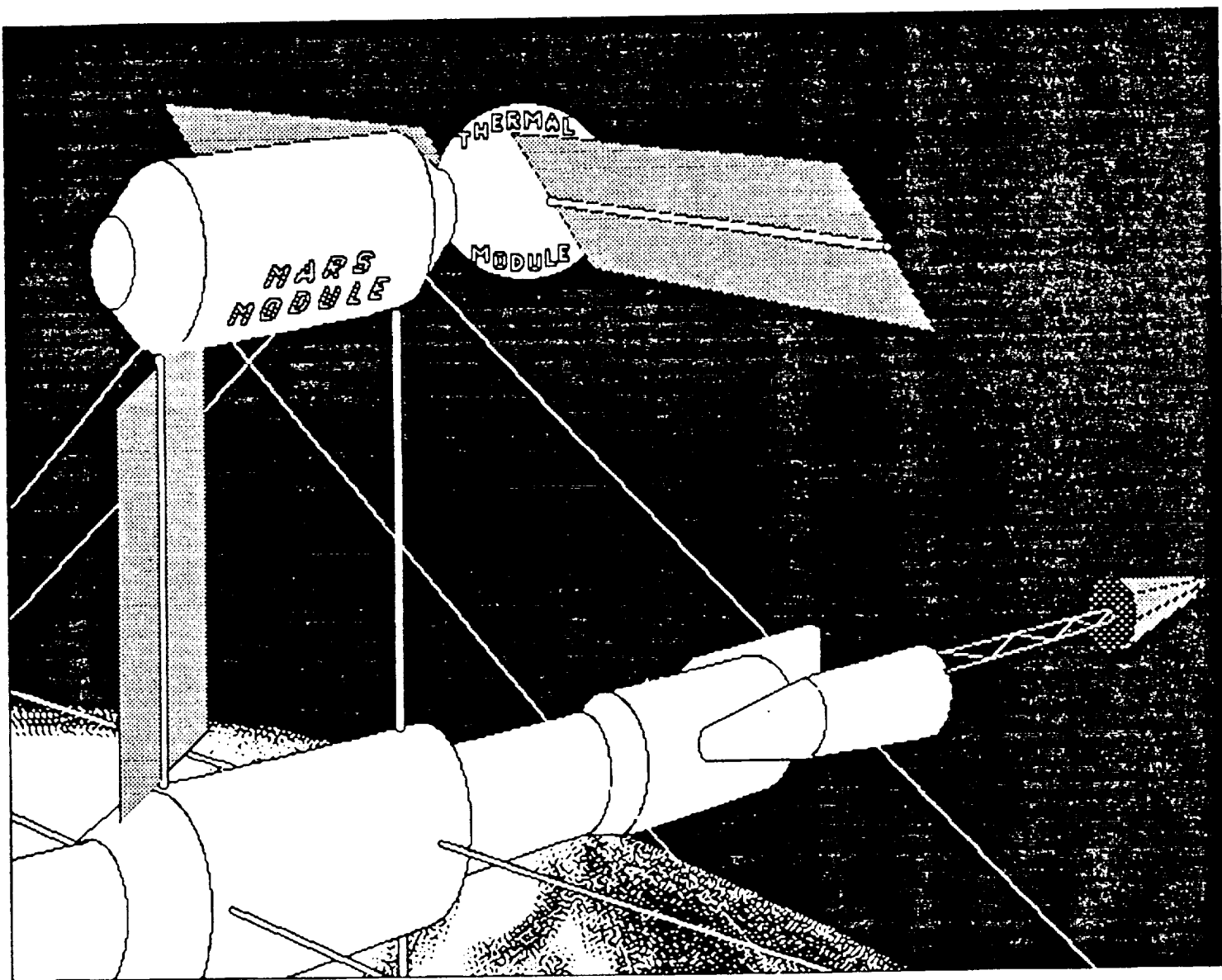
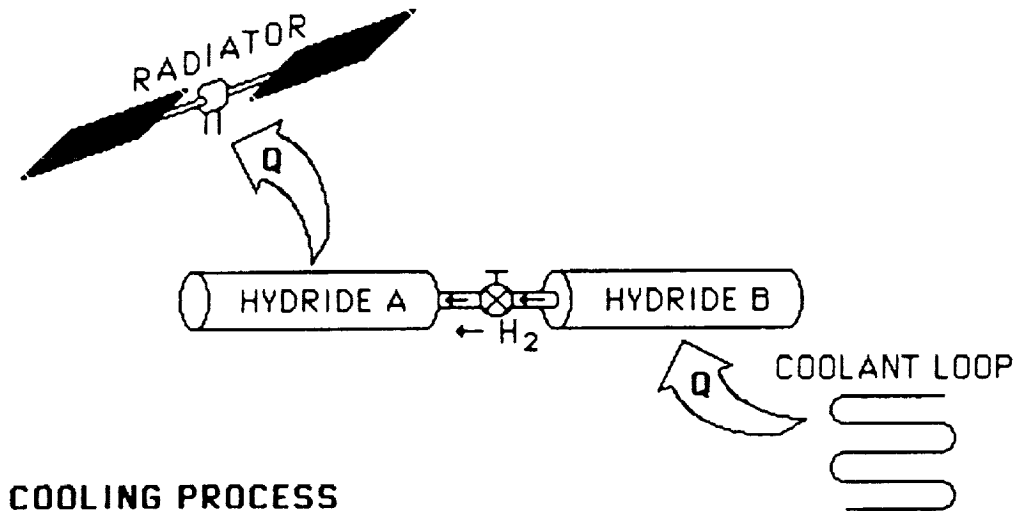
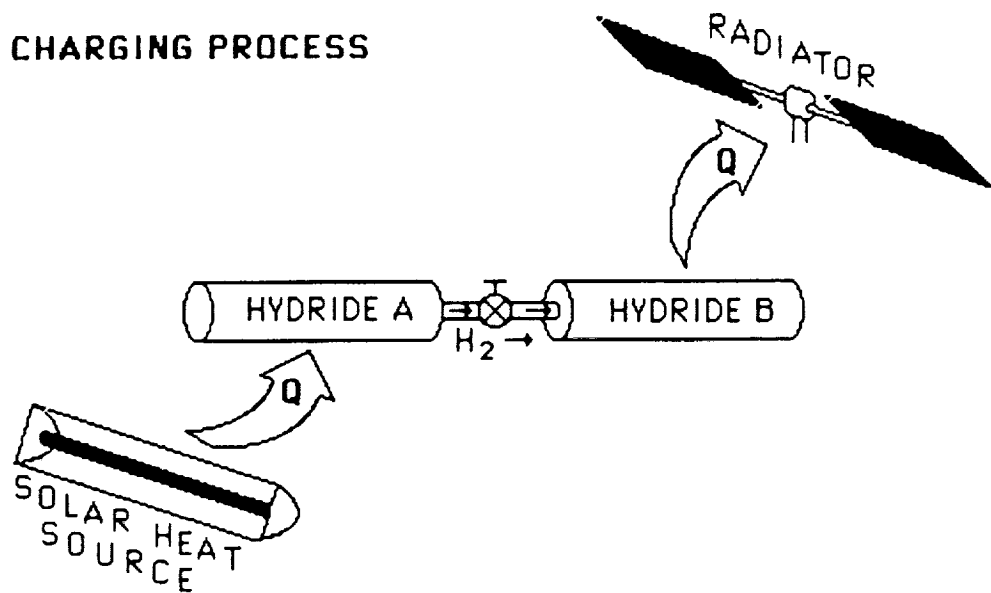


Figure 4-1. Mars-bound spacecraft in final assembly and checkout phase in LEO receives supplementary cooling from a detachable accessory thermal system. A metal hydride heat pump in the thermal system module extracts heat from the Mars module's equipment loop and rejects it via steerable radiators.

CHARGING PROCESS



COOLING PROCESS

Figure 4-2. Illustration of the heat flow in a hydride heat pump for an LEO auxiliary thermal system, such as Fig. 4-1.

A solar thermal powered heat pump cycle for an LEO auxiliary thermal system would resemble Figure 4-3. The cycle begins in the upper right hand corner of the figure at Point 1, where a 134°C (273°F) solar thermal heater supplies heat to hydride A. At that temperature, hydride A's equilibrium pressure is 1960 kPa (284 psia). Hydride B is in thermal contact with a 48°C (118°F) radiator at this time, and its equilibrium pressure is 980 kPa (142 psia). The ratio of the two hydrogen pressures is 2:1. This pressure ratio will cause hydrogen to flow from hydride A to hydride B if the valve between the two is opened (see Figure 2-5). Typical hydride heat exchanger designs (ca. 0.5 inch tubes) will permit the transfer of 90% of the total hydrogen content from A into B in about 600 seconds under these conditions.

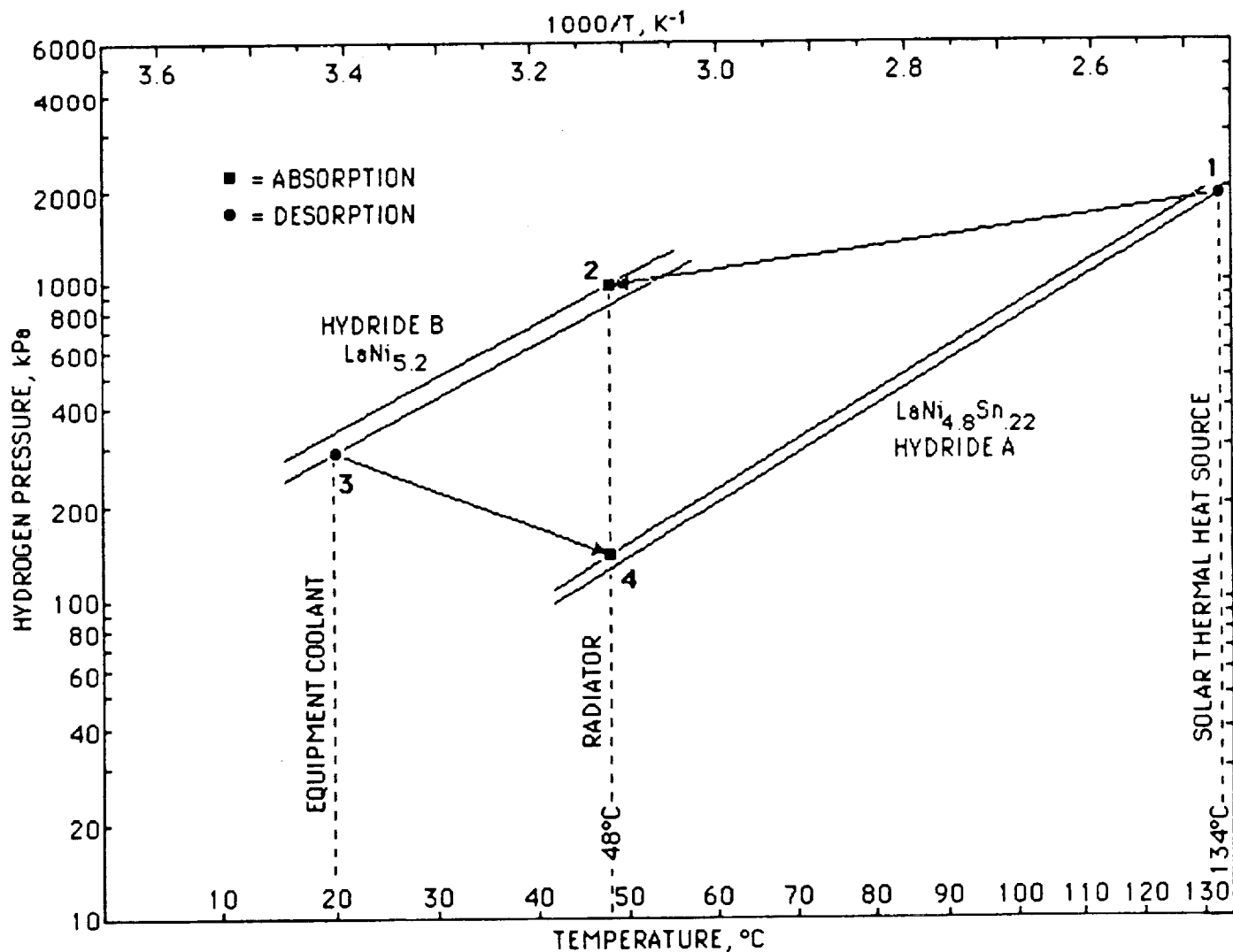


Figure 4-3. Equilibrium pressure-temperature diagram of a solar thermal powered metal hydride heat pump for an LEO auxiliary thermal system.

The transfer of hydrogen from hydride A, at point 1, to hydride B, at point 2, increases the chemical potential energy of the hydride pair. The work needed to accomplish this comes from absorbing heat at a higher temperature (134°C) and rejecting heat at a lower temperature (48°C). During this part of the process, the system performs like a heat engine. The dynamic transfer of hydrogen from A to B does not occur at the nominal equilibrium pressure-temperature conditions at points 1 and 2. The pressure throughout the system will be virtually constant during process 1-2, somewhere between 1960 kPa and 980 kPa (computer model HAWK predicts about 1400 kPa). Hydride containers A and B will have temperature gradients inside them, A being cooler than the heat source and B being warmer than the radiator.

Hydride B is subsequently connected to a 20°C (68°F) coolant loop, such as the equipment loop in a Mars module. This corresponds to equilibrium point 3 in Figure 4-2. At 20°C, the equilibrium hydrogen pressure of hydride B is 290 kPa. Hydride B extracts heat from the 20°C equipment loop as it releases hydrogen. At this time, hydride A is thermally connected to the radiator at 48°C (118°F) and its equilibrium pressure is 145 kPa. Hydride A's nominal equilibrium condition is represented as point 4 in Figure 4-2. The equilibrium pressure ratio during the transfer process is 2:1. The dynamic operating pressure-temperature coordinates are displaced from points 3 and 4 by ΔP s and ΔT s that promote chemical reaction and heat transfer.

Computer simulations of 90% complete hydrogen transfer between a pair of state-of-the-art hydride containers indicate that the hydride heat pump cycle of Figure 4-3 could operate at a rate of one round-trip cycle every 20 min. Several smaller units operating in parallel would be needed to extract heat from the Mars Module at a steady rate. Each kW of heat flow extracted would require about 13 kg of alloy. Adding the mass of the containers (wet), the estimated heat pump mass is 16 kg per kW of cooling power. The solar collector (ca. 1 m² of planar array per kW at 407 K, see Fig. 3-1) would add to the total mass of the accessory thermal system.

Detailed trade-off studies would be needed to determine the merit of adding the mass of the heat pump and solar collector to reduce the radiator area. The particular operating conditions of Figure 4-3 led to a 20 minute heat pump cycle. If the solar thermal heat source were replaced by heat at higher temperature (e.g., concentrated solar or nuclear waste heat) faster cycles and lighter hydrides, such as MgH₂, would be possible. The following example considers the use of waste heat from an RTG to power a MgH₂ vs. FeTiH metabolic cooler.

4.2 HYDRIDE COOLER BASED ON LUNAR MATERIALS.

The rare earth nickel hydrides used in the preceding example could be manufactured from lunar minerals that are relatively diffuse. Other types of hydrides could be obtained from abundant lunar materials. Typical lunar soil contains about 5 wt % ilmenite, FeTiO₃ (Williams, et al., 1979). Apollo 15 "green clods" (about 17 wt % MgO) represent up to 20 percent of the soil by volume in some locations (Taylor, 1975). These minerals could be refined on the moon to produce oxygen for propulsion and life support, and metals for hydride thermal devices. The metal reactants account for most of the mass of a hydride subsystem, so the mass transported from Earth (heat exchangers, controls, etc.) would be significantly reduced.

Figure 4-4 shows the relationship of the components for a hydride cooler, powered by waste heat from a nuclear power system. The hydride draws heat from the cooling fins of a radioisotope thermoelectric generator (RTG), rejects heat to an auxiliary radiator panel, and supplies coolant to the thermal control system of a lunar base. The larger cross-hatched lines carry heat transfer fluids. The smaller lines carry hydrogen. Two A-B pairs of hydrides operate in an asynchronous cycle to provide a steady flow of coolant. The relative placement of the components in Figure 4-4 is for conceptual purposes only. The RTG might be located in a small crater for shielding purposes and the other components could be placed outside the rim of the crater.

Figure 4-5 maps a plausible cooling cycle. Process 1-2 is the recharge process, during which chemical potential energy is stored. At point 1, heat is supplied to MgH_2 in an A module at 450°C (842°F) as it desorbs hydrogen. The enthalpy of the desorption reaction, $\text{MgH}_2 \rightarrow \text{Mg} + \text{H}_2$ is 75 kJ/gram-mole (16,100 Btu/lb) of H_2 desorbed. Waste heat is intercepted, on its path from the cold shoe of the thermoelectrics to the RTG's radiator, by the fluid loop. At point 2, the hydrogen flows into a B module at 53°C (127°F). The enthalpy of the absorption reaction, $2\text{FeTi} + \text{H}_2 \rightarrow 2\text{FeTiH}$, is 28 kJ/gram-mole (6030 Btu/lb) of H_2 . This heat is dissipated through a lower temperature portion of the auxiliary radiator area.

After process 1-2 is complete, an A module is cooled by the auxiliary radiator from point 1, 450°C (842°F), to point 4, 286°C (547°F), in Figure 4-5. At the same time, a B module cools itself from 53°C (127°F) to 6°C (43°F) by desorbing a fraction of its hydrogen content adiabatically. This moves hydride B from point 2 to point 3 in Figure 4-5. Cooling process 3-4 begins when fluid from the refrigeration load (a lunar base metabolic cooling loop?) starts circulating through a B module. Each gram-mole of hydrogen gas (4.4×10^{-3} lb) desorbed from a B module, by the reaction $2\text{FeTiH} \rightarrow 2\text{FeTi} + \text{H}_2$, corresponds to 28 kJ (27 Btu) of cooling. The gas flows to an A module where it is absorbed, by the reaction $\text{Mg} + \text{H}_2 \rightarrow \text{MgH}_2$, releasing 75 kJ (71 Btu) of heat to the auxiliary radiator for each gram-mole of H_2 absorbed.

The objective of this active cooling process is to reduce radiator area, and consequently to reduce the mass and volume of equipment transported from Earth. To gauge the benefits of heat pumping at the peak of the solar day, it is assumed that all radiators are lain flat on the surface of the moon, have a solar absorptivity, $\alpha_s = 0.10$, and an infrared emissivity, $\epsilon_{\text{ir}} = 0.75$.

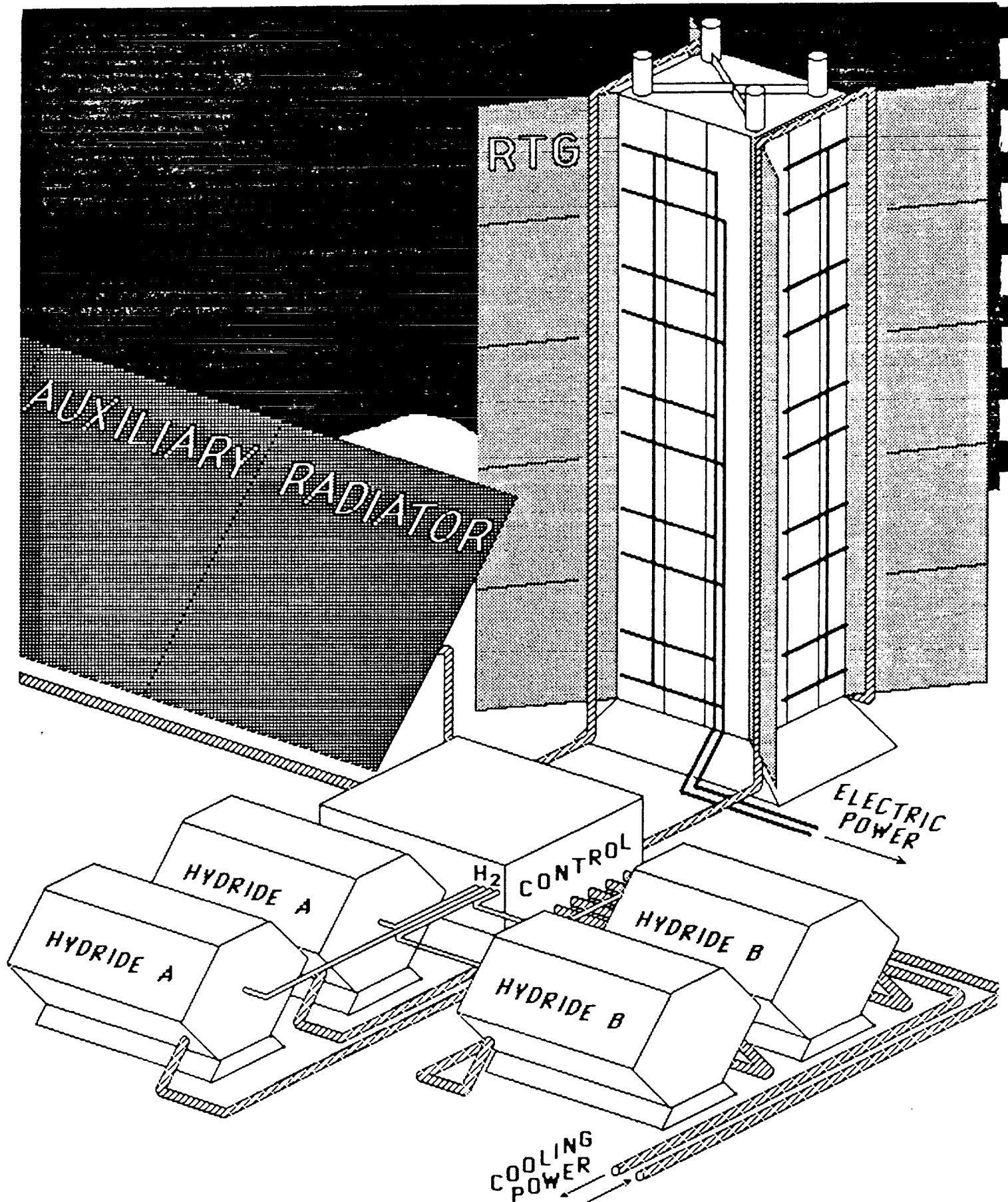


Figure 4-4. Waste heat from a nuclear thermoelectric generator powers a metal hydride cooler for a lunar thermal control system.

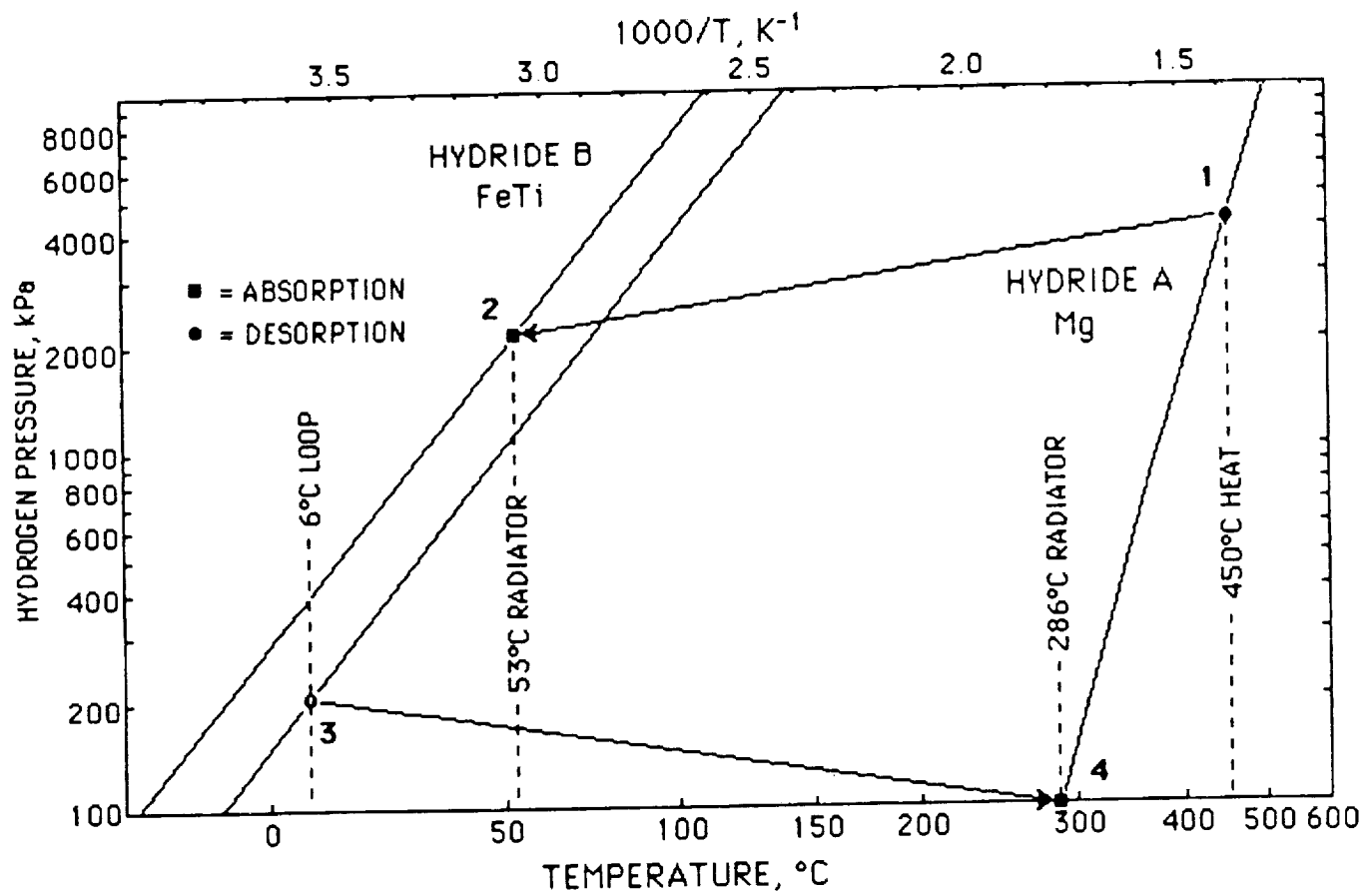


Figure 4-5. Metabolic cooling cycle pumps heat from a 6°C (43°F) water loop to a 53°C (127°F) radiator. The cycle is powered by waste heat from an RTG at 450°C (842°F) with heat rejection at 286°C (547°F). FeTi Mg are abundant in lunar minerals.

Neglecting nearby tall structures and mountains, a vertical facing radiator only "sees" the sun and black space (ca. 0 K). Therefore, each m² of radiator will reject heat at a rate that is related to radiator temperature, T_r , as follows:

$$\begin{aligned}\dot{Q} &= \alpha_s I_s - \sigma \epsilon_r T_r^4 \\ &= 0.10 (1352 \text{ W/m}^2) - (5.6697 \times 10^{-8} \text{ W/m}^2 \text{ K}^{-4}) (0.75) T_r^4\end{aligned}$$

where I_s is the nominal solar intensity and σ is the Stefan-Boltzmann constant.

Direct radiation of the 6°C (43°F) cooling load could have been accomplished at a heat flux of 123 W/m² (39 Btu/hr-ft²). An active 6-member crew might produce about 1800 W (6137 Btu/hr) of metabolic heat, so 14.6 m² (158 ft²) of radiator area would be needed.

The thermally powered heat pump described above could handle the same 1800 W heat load with 5.2 m² (56 ft²) of radiator at 53°C (127°F) and 1.2 m² (13 ft²) of radiator at 286°C (547°F). The total radiator area, 6.4 m² (69 ft²) is just 44% of the direct radiation case.

The comparison becomes even more attractive if radiator degradation is considered. Assuming that emissivity remains constant at $\epsilon_{ir}=0.75$, degradation of solar absorptivity beyond $\alpha_s=0.19$ would make direct radiation of a 6°C heat load from radiators spread on the lunar surface infeasible during periods of peak insolation. The structures and mechanisms of steerable radiators would enter the mass comparison with degraded radiator performance. If the hydride heat pump radiators were degraded to $\alpha_s=0.19$, simple surface mounted radiators could still be used by increasing the total surface area from 6.4 m² (69 ft²) to 9.2 m² (99 ft²).

The estimated mass of the metal hydride heat pump is strongly affected by its cycle rate. Computer program HAWK is not currently capable of simulating MgH₂ formation and decomposition because the process is different from the lower temperature hydrides for which the model was developed. The literature indicates that the sorption rates will be slower than rare earth pentanickel or iron titanium hydrides but further development will be needed to gain accurate predictions of the dynamics of heat transfer and chemical kinetics in MgH₂ containers. For the sake of very rough estimation, assume that the heat pump cycle of Figure 4-5 requires 40 minutes to complete. Each of the two B modules would be on line for about 20 minutes and during that time 1800 W would be extracted from the coolant loop. The total heat input would be 2.16 MJ (2049 Btu) requiring 77.1 gram-moles of transferrable H₂ capacity. If 90% of the hydrogen is transferrable within the 20 minute period, the total hydrogen capacity of each B module would be 85.7 gram-moles or 173 grams (0.38 lb). The mass of FeTiH needed to contain this amount of hydrogen is 18 kg (40 lb) and, adding 25% for the container and heat transfer fluid, each B module would weigh about 23 kg (50 lb).

The A modules would be much lighter because MgH₂ has more than seven times the gravimetric hydrogen content of FeTiH. The MgH₂ mass needed to

absorb the 173 grams of hydrogen flowing from a B module is 2.3 kg (5 lb). The container and heat transfer fluid are a larger fraction of the mass of an A module than a B module, owing to the reduced density of MgH_2 . The total mass of an A module is estimated at 7 kg (15 lb).

The heat pump subsystem, comprized of two A modules and two B modules, would have a total mass of 60 kg (130 lb), plus the mass of the valves and other control components and fluid lines. FeTi accounts for 60% of the total heat pump mass so, if the alloy were produced as a by-product of a lunar oxygen plant, only 24 kg (53 lb) would need to be transported from Earth. The system volume would be approximately 28 liters (1 ft³).

4.3 HYDRIDES AND MOBILITY

In the preceding example, a metabolic heat pump for a crew of six was estimated at 60 kg (130 lb) and 28 liters (1 ft³). The heat pump completed a cycle every 20 minutes, drawing power from a stationary nuclear heat source. It is also possible to provide very compact hydride thermal control subsystems for EMU's, rovers and other mobil life support systems, where large radiators are not feasible. Some mobil applications have a heat source that could be used to drive a heat pump cycle just like the preceding example. A fuel cell powered rover might be designed with a relatively high operating temperature so that waste heat from the fuel cell could be rejected from a small radiator. A portion of that waste heat could be used to power a hydride heat pump.

Other mobil life support systems may be battery powered and have no waste heat available to power hydride cycles. In that case it is possible to separate the hydrides from the heat source by designing a cycle that has the features of both a heat pump and a thermal storage device. The metal hydride heat pump (MHHP) for advanced Space Station EMUs, currently under development for JSC (NAS 9-17819), employs these operating principles. Figure 4-6 is a sketch of the MHHP showing two hydride containers that operate in a thermal cycle that is similar to the LEO and lunar examples in sections 4.1 and 4.2. The most important difference between the MHHP and the preceding examples is that the process is divided into two distinct phases. Only the two hydride containers and a small radiator are attached to the EMU during extravehicular activity (EVA). The thermal energy and auxiliary cooling equipment, needed to recharge the MHHP, are supplied by the Space Station.

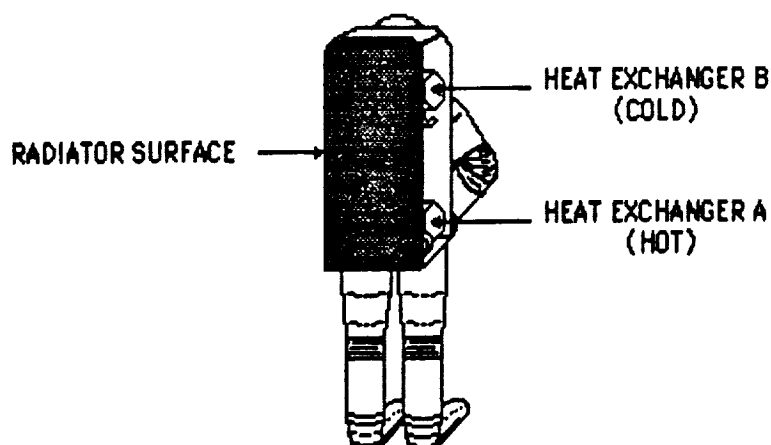


Figure 4-6. Major components of a MHHP for an advanced Space Station EMU. The two heat exchangers contain metal hydride alloys.

The hydride in heat exchanger B extracts heat from the liquid coolant of the EMU at temperatures as low as 4°C (40°F) while flowing hydrogen to the hydride in heat exchanger A. The hydride in heat exchanger A absorbs the flow of hydrogen, dissipating heat to the radiator at temperatures up to 42°C (108°F). The recharge process takes place after the EVA is complete. Hydride A is heated to 93°C (200°F) by a heat source on the Space Station while heat is rejected from hydride B at 25°C to a coolant loop. The cycle is shown in Figure 4-7. The EVA and recharge processes take place over periods of hours, so the pressure ratios (PRs in Fig. 4-7) are smaller than the rapid-cycling heat pumps in Figures 4-3 and 4-5.

The most severe environment encountered during this study for EMUs, rovers and other mobile equipment is the surface of the Moon. During the peak of the lunar day, surface temperatures reach 405 K (170°F). A vertical surface, such as the backpack of an EMU will receive several hundred W/m² of IR and albedo flux in addition to solar irradiation. Some of the objectives of a lunar base depend upon an uncontaminated atmosphere, so venting from sublimators will probably be disallowed. Hydride heat pumps would be a prime alternative for thermal control in lunar EMUs and rovers.

A metabolic cooling cycle based on hydrides manufactured on the Moon was presented in Figure 4-5. The same hydrides could be used to provide heat pumping/thermal storage for a battery-powered shirtsleeve rover. Figure 4-8 shows a vehicle (Walligora and Sedej, 1986) that provides mobility and permits two crewmembers to work without the restrictions of a pressure suit and pack-mounted PLSS.

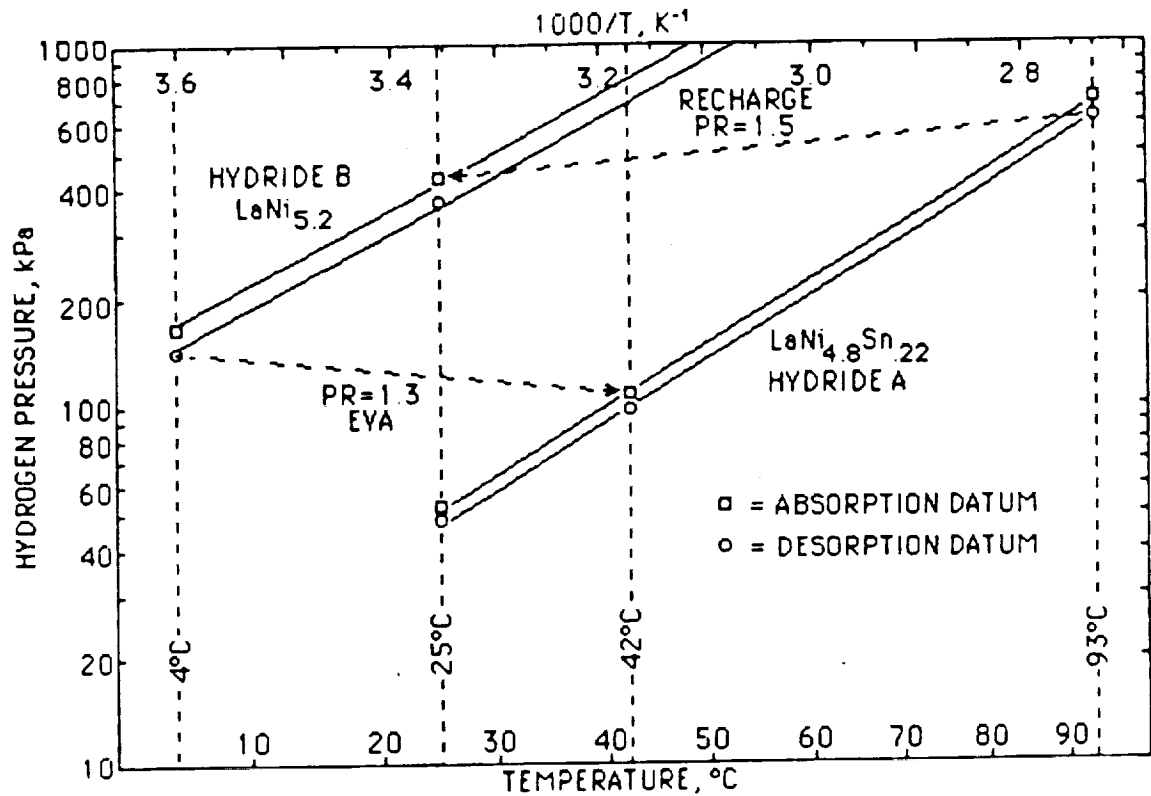


Figure 4-7. Heat pump cycle for an advanced Space Station EMU.

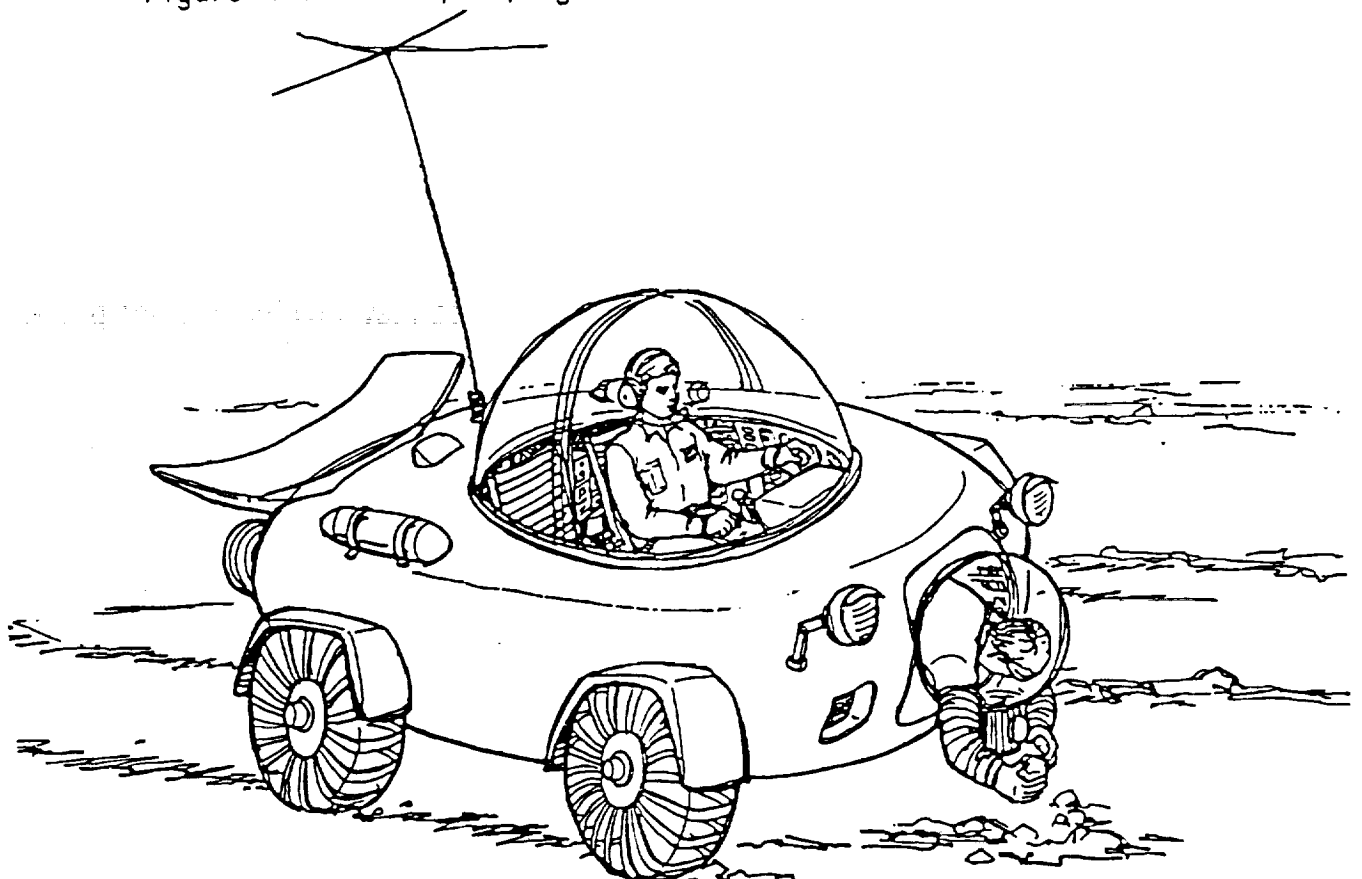


Figure 4-8. Transportation with pressurized volume and anthropometric suit extension (after Waligora and Sedej, 1986).

Suppose that an active crew of two remains aboard the rover for a period of eight hours. The metabolic cooling requirement would total to about 17 MJ (16,400 Btu). In scaling the previous result from section 4.2 it is necessary to recognize that continuous heat pumping is not required in the present example. Like an EMU, the vehicle stands idle for a period of several hours at the end of an excursion while the batteries and life support equipment are serviced. Since there is no need for two parallel units operating out of phase with one another, the mass and volume per unit of heat pump capacity are only half that calculated in section 4.2. The thermal capacity is much larger however, so the mass of the hydride subsystem grows to 236 kg and its volume to 110 liters (4 ft³). As before, these hydrides are potentially available from lunar resources so only a fraction of the system mass would need to be transported from Earth for use at advanced bases.

Only 0.4 m² (4.3 ft²) of 286°C (547°F) radiator would be required to reject heat from hydride A. The radiator should be placed on a horizontal surface at a location that could not be touched accidentally during EVA. The 53°C (127°F) radiator, needed for regeneration of the heat pump, would remain at the service depot since it is not used during the excursion.

In summary, the same advantages perceived by JSC Thermal Systems Branch staff in their MHHP concept for the Space Station EMU, pertain to all mobile life support systems in thermal environments that are too hot for reasonably small radiators to carry low temperature heat loads.

4.4 HYDRIDE THERMAL POWER TRANSMISSION

Future spacecraft and lunar or planetary bases may involve nuclear power, concentrating solar dynamic power or power system alternatives that have not yet been conceived. Because of heat and/or nuclear radiation, it may be infeasible to locate a habitat very near to the power source. Electric power can be transmitted through cables over reasonable distances without much loss, but thermal power transmission is a greater challenge. The reason for using waste heat to power thermal control systems is to conserve electricity. If the point of use is too far from the heat source, the heat loss and pumping power demand of a pumped liquid loop will negate the advantages of thermal power.

Hydrogen gas is the least viscous fluid known. A larger volume flow of hydrogen can be transmitted through a pipe of a given diameter and length, at a given pressure, ΔP , and temperature, than any other gas. The preceding

examples have shown pairs of hydrides (A and B) in close proximity, exchanging hydrogen in thermal cycles. The short distances between hydrides A and B in these examples is not a necessary condition. The only physical linkage that is necessary between two hydrides is a gas line. The length of the gas line is relatively unimportant* so long as the pressure drop is negligible. Therefore, thermal power from a heat source can be transmitted over long distances by placing hydride A near the heat source, hydride B in some remote thermal control system, and flowing hydrogen back and forth through a long gas line between the two. The effect is that of a chemical heat pipe wherein thermal energy is transmitted in the form of chemical potential energy.

One potential application for transmitting thermal power in this way is shown in Figure 4-9. Hörz (1984) has discussed the possibility of using lunar lava tubes as habitats because they offer natural shelter from cosmic and solar radiation and provide a nearly constant temperature environment. The thermal design of such a habitat would be relatively simple, compared to surface structures that must withstand the large diurnal temperature swings.

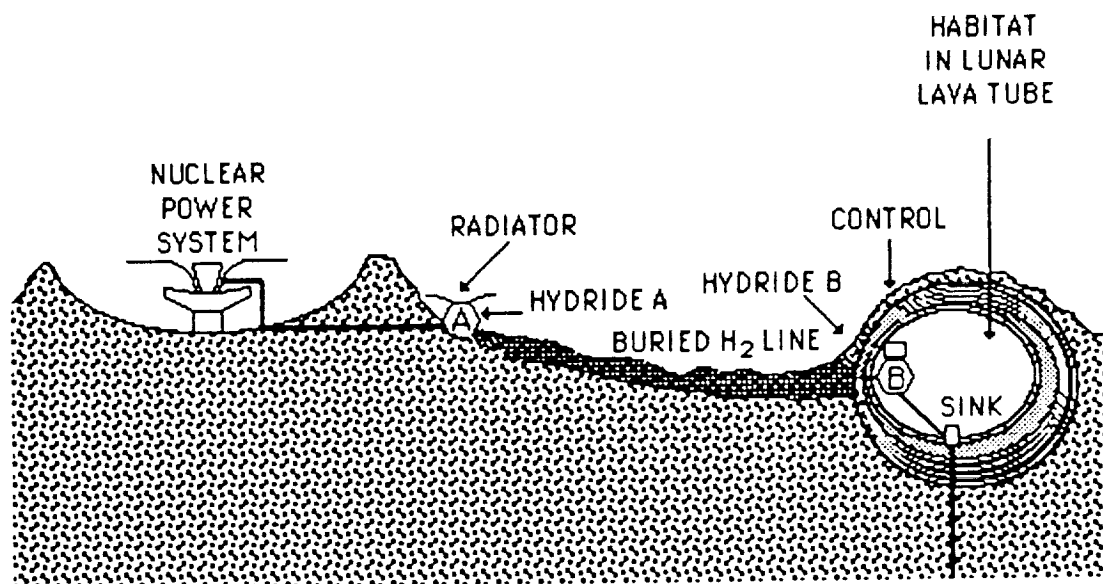


Figure 4-9. Hydride heat pumps can be located some distance from the heat source that powers them.

*The internal volume of the gas line between two hydrides is pressurized and depressurized on each cycle. This results in an irreversible work term in a detailed thermodynamic analysis of the cycle, so the volume of the line should be small, relative to the total volume of hydrogen that passes through the line.

The average internal heat load in the habitat might be balanced by a controlled heat leak through a moderate insulation barrier to the walls of the lava tube (ca. -20°C or -4°F). Any active control required to offset heat load variations could be accomplished with a hydride heating/cooling subsystem.

Thermal power to operate the heat pumping and refrigeration cycles might be drawn from a power system at a remote location. Hydride A, and enough auxiliary radiator to cool it, might be located near the power system. A small hydrogen line*, buried deep enough in the lunar regolith to protect it from damage by micrometeorites or surface vehicles, could flow hydrogen to and from hydride B, located near the habitat. Hydride B, in Figure 4-9, is connected to a heat sink that rejects heat to subsurface rock (see section 3.3). It may be more convenient, in some cases, to use a surface-mounted radiator.

Figure 4-9 is offered as a simple example of how hydrides might contribute to the efficient use of thermal resources at a lunar base. The particular details of this example are unimportant. The point to be made here is that hydride subsystems could transmit thermal power over respectable distances without heavily insulated lines or pumping power penalties.

4.5 SYNERGISM BETWEEN HYDRIDES AND OTHER SUBSYSTEMS

The main focus of this study has been the use of hydrides in advanced thermal control systems for future space activities. During the course of the study however, several opportunities to use hydrides for other purposes became apparent. In some cases hydrides could serve as thermal control subsystems at the same time as they provide other valuable functions. These additional uses of hydrides contribute to their attractiveness as thermal control alternatives because a portion of the mass and volume can be written off against the secondary function.

HYDROGEN/HEAT BUFFER

Consider Figure 4-10 for example; a rover with cryogenic $\text{H}_2\text{-O}_2$ reactant storage, a fuel cell for power, and a thermal system for fuel cell cooling. A metal hydride reservoir could serve dual purposes in this system.

* A 2.5 cm (1 in.) I.D. tube could carry 100 kW of chemical potential energy over a distance of several hundred meters without significant pressure drop.

Lightweight cryogenic hydrogen storage containers generate a minimum flow of boil-off gas that must be either consumed by the fuel cell, stored or vented. A hydride could absorb boil-off during periods when the fuel cell's demand is less than the boil-off rate. At some later time, when the fuel demand exceeds the boiloff rate, the hydride could discharge its gas content to the fuel line, thereby reducing the need to vaporize LH_2 .

The heat flow to and from the hydride is also complementary to the operation of the thermal system. Excess boil-off occurs when the fuel demand is low and the fuel cell's heat input to the thermal system is also low. Therefore, the heat generated as the hydride absorbs gas is dissipated to the radiator at a time when it has excess capacity. Later, when the hydrogen demand and fuel cell heat rejection are high, the hydride extracts some of the heat as it desorbs the stored gas, thus reducing the heat load on the radiator.

The overall effects of the heat/hydrogen buffer on the rover are reduced H_2 storage mass and volume (through boiloff control) and a smaller radiator (by reducing the peak heat load).

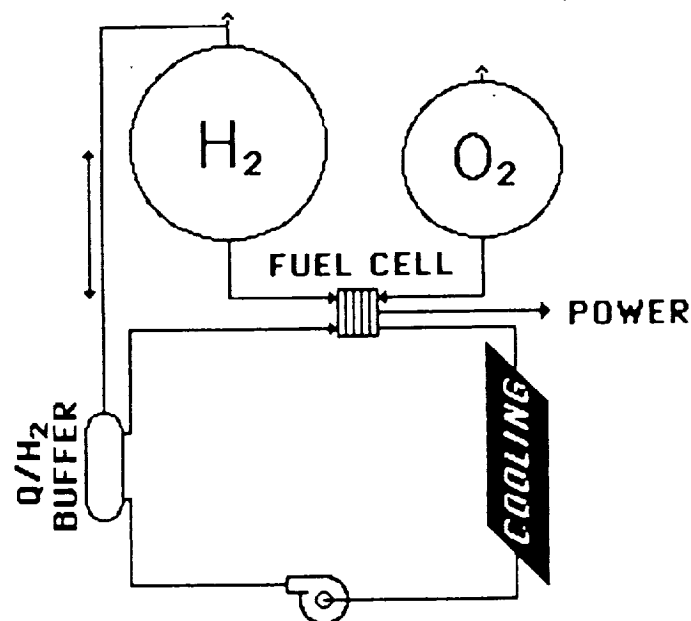


Figure 4-10. Hydride H_2 /heat buffer interacts with fuel storage and thermal systems in a cryogenically powered rover.

HYDRIDES FOR THERMAL CONTROL AND SHIELDING

Crews and sensitive instrumentation on extended missions outside of Earth's protective magnetosphere will require protection from solar particles, cosmic radiation and probably radiation from nuclear power systems. Neither the Moon nor Mars has a significant magnetosphere so habitats and work environments will be covered with soil or located in natural caves, lava tubes or man-made tunnels. Spacecraft that are manned for extended periods, and surface vehicles that are used frequently at lunar and planetary bases will also require protection. Materials that are effective for attenuating radiation and blocking particles are necessarily massive and will be a major factor in the design of shielded systems. Thermal control systems will also contribute strongly to the masses of spacecraft and surface vehicles. Metal hydrides can serve, both as thermal control system materials and as shielding, so it is attractive to consider ways to reduce overall mass by combining these capabilities into one dual purpose subsystem.

One of the principle metal hydride research objectives of the late 1950s and early 1960s was the evaluation of metal hydrides as lightweight nuclear shielding materials (Mueller et al., 1968). Currently proposed shielding for the SP-100 space nuclear power system consists of layers of lithium hydride and tungsten (Barrattino et al., 1986). Preliminary work at HCL with simple calculations for monoenergetic neutron and gamma radiation fluxes indicates that metal hydride systems, such as those discussed throughout this report, have potential as shielding. Preliminary comparative calculations of shielding effectiveness for typical metal hydrides, their parent alloys, and typical hydride container materials are presented in Table 4-1, along with the two presently proposed SP-100 shielding materials. The approximations used are the very simple ones of the neutron removal cross-sections. Table 4-1 was prepared using the 8 MeV neutron flux data of Chapman and Storrs (1955) and the constant mass attenuation coefficient for gamma flux, which approaches the constant value of $0.0065 \text{ m}^2/\text{kg}$ at 1 MeV for a variety of metals and compounds (Glasstone and Sesonske, 1981). Forty percent of the container volume was assumed to be void space in the hydride powder. The table indicates that metal hydrides, their parent alloys, and containers may serve as shielding materials against both solar proton events and isotropic cosmic radiation.

Figure 4-11 shows a pair of hydrides, A and B, located in the outer walls of a compartment. The hydrides would exchange hydrogen, performing the active thermal control processes discussed previously in this report, and providing shielding against various types of radiation and particle bombardment.

TABLE 4-1. Comparison of metal hydrides, parent alloys and containment materials with state-of-the-art shielding for the SP-100.

Percent incident 8 MeV neutrons attenuated (%NA) and percent incident 1 MeV gammas attenuated (%GA) by 0.01 m (0.4 in) thickness, (equal volume basis); and by $0.01/\rho$ m thickness (with ρ the density in Mg/m^3), (equal mass basis). Neutron attenuations computed by the removal cross-section approximation (Glasstone and Sesonske, 1981; Chapman and Storrs, 1955), and gamma attenuations computed by the constant mass attenuation coefficient approximation (Glasstone and Sesonske, 1981).

Material	$\rho(\text{crystal})$ (Mg/m^3)	T(melt) ($^{\circ}\text{C}$)	% Solid density in possible shield layer(s)	%NA equal vol basis	%NA equal mass basis	%GA equal vol basis	%GA equal mass basis
*W	19.35	3407	100	15	1	72	6
Al	2.70	660	100	8	3	16	6
Fe	7.86	1536	100	15	2	40	6
*LiH	0.780	680	100	11	14	5	6
**VH _{0.94}	5.62	-	47	8	3	16	6
**VH ₂	4.52	-	60	11	4	16	6
**LaNi ₅	8.27	1350	47	6	2	22	6
**LaNi ₅ H ₆	6.59	-	60	9	2	23	6
**Mg	1.74	649	46	3	3	5	6
**MgH ₂	1.45	-	60	6	7	6	6
U	19.0	1132	36	6	1	36	6
UH ₃	11.4	-	60	11	2	36	6

* presently proposed shield materials for SP-100

** V, La, Mg removal cross-sections approximated by $\sigma_r = 0.35 A^{0.42}$, in barns (10^{-28} m^2), with A the atomic weight (Glasstone and Sesonske, 1981).

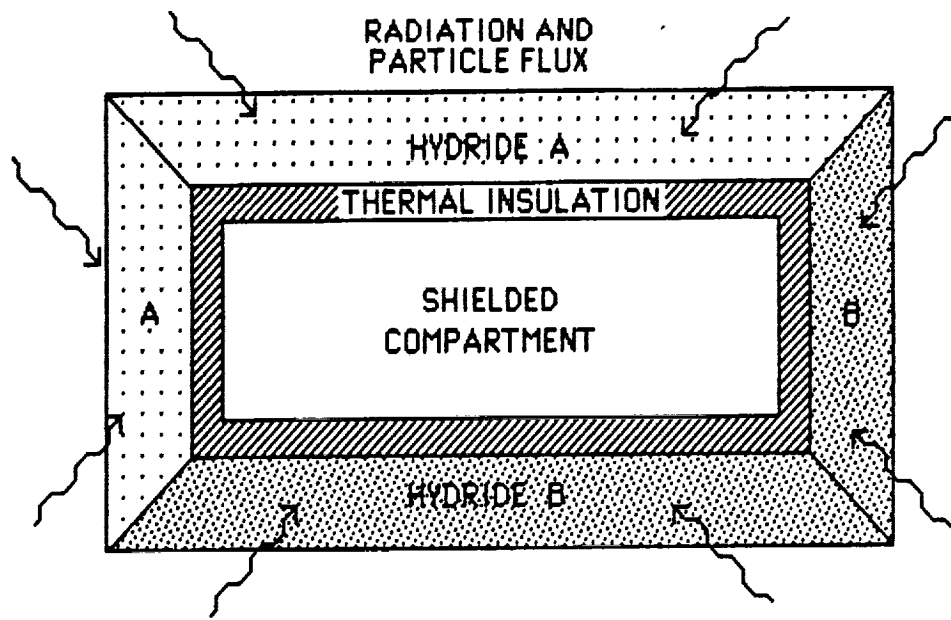


Figure 4-11. Active thermal control subsystem, comprised of hydrides A and B, doubles as shielding against radiation and particles.

5.0 SUMMARY AND CONCLUSIONS

Metal hydride heat pumps and thermal storage devices may enhance the performance of thermal systems in future space activities in several ways. Their most useful features are the following:

- Hydride heat pumps can increase heat rejection temperatures and thereby reduce radiator area.
- Ability to use thermal power (solar or waste heat) instead of electricity, reduces power-mass penalties
- Hydride thermal subsystems are very simple--some thermal subsystems may have no moving parts, except those associated with external fluid circulation.
- The problems of zero-g liquid acquisition that complicate liquid-vapor alternatives do not affect hydrides.
- Hydrides are competitive with the best alternative thermal storage materials on a mass basis.
- Hydrides are the most compact nonventing thermal storage alternative.
- Hydride heat pipes can transmit thermal power over long distances without insulated lines or excessive pumping power.
- The raw materials for producing several useful hydride alloys are available on the Moon and Mars.
- *Commonality* advantages emerge when hydride thermal devices are used in systems that involve hydrogen storage.
- Hydrides are effective radiation shield materials so hydride thermal devices may double as shielding.

Heat pumping makes it possible to implement refrigeration systems and reject low temperature heat loads with simple nonsteerable radiators (e.g., roll-out lunar surface radiators) even when those radiators are in a degraded state. Electrically powered heat pumping is sometimes infeasible because, although the radiators are made smaller and/or simpler, the increased mass of the electric system negates the advantages. Hydride heat pumps and refrigerators are thermally powered. The only electric power needed is for circulating heat transfer fluids and for control.

Hydride heat pumps are intrinsically simple. It is possible to design a hydride heat pump with no moving parts other than hydrogen molecules. Two

container/heat exchangers may be connected by a gas tube and exposed alternately to heat sources and sinks to perform heat pumping and refrigeration functions. An optional throttling valve in the hydrogen line adds control flexibility. The only other components are those associated with interfacing the hydride heat pump with heat sources, fluid loops, radiators, etc. Some hydrides have a demonstrated ability to perform through many thousands of cycles of absorption/desorption without significant changes in performance.

The operation of hydride thermal subsystems is unaffected by microgravity because the gas phase (hydrogen) can only "condense" in the presence of the solid metal powders in the hydride containers. There are no liquid phase acquisition or transport problems.

Hydrides are among the best phase change thermal storage media in terms of mass, and they are superior in terms of volume to other nonventing alternatives. This allows very compact thermal subsystem designs that are especially useful in mobile applications such as EMU's and rovers. Hydrides are one of the few thermal storage materials that could be produced from resources found on the Moon and Mars.

The extensive projected use of nuclear power systems in future space activities presents a number of attractive possibilities for thermally powered hydride subsystems. A prime possibility is that of transporting heat from nuclear reactors over long distances by a form of hydride heat pipe. Chemical potential energy transmission in a small hydrogen line would be much more efficient than pumping heat transfer fluids over the same distance. The value of hydrides as shielding materials also contribute to the synergistic possibilities of using hydrides in conjunction with nuclear power systems

The relatively cold environment, and the abundance of CO₂ and water on Mars presents opportunities to simplify many thermal subsystems with shuttle-like sublimation coolers that vent the vapor phase to the martian atmosphere. This limits the applicability of hydrides on the surface of Mars, but the usefulness in Mars orbit, on the surfaces of Phobos or Deimos, or on Earth's Moon is similar to other space applications where venting is not permissible.

Surface bases on the Moon, Mars, Phobos or Deimos also present the possibility of rejecting heat to subsurface rock by conduction. Preliminary analyses indicate that a few hundred watts per square meter could be dissipated into a small diameter hole drilled into a typical basalt formation.

6.0 REFERENCES

- Alter, D. and Clemmshaw, C.H., *Pictorial Astronomy*, Thomas Y. Crowell Company, New York (1956).
- Babb, G.R. and Stump, W.R., "Mars Orbit Selection": In NASA (June 1986),
- Bankston, C.P. and Shirbacheh, M., "AMTEC" High Efficiency Static Conversion for Space Power": *ibid.*
- Barrattino, W.J., El-Genk, M.S., and McDaniel, P.J., in *Space Nuclear Power Systems* 1985, El-Genk, M.S., and M.D. Hoover, eds., Orbit Book Co., Malabar, FL (1986).
- Blacic, J.D., Rowley, J.C., and Cort, G.E., "Surface Drilling Technologies for Mars," in NASA (June 1986), *op cit.*
- Buden D. and Angelo J.A., "Nuclear energy -- Key to Lunar Development": in Mendell, W.W. ed., *vide infra.*
- Burke, J.D., "Merits of A Lunar Polar Base Location": *ibid.*
- Canjar, L.N., Pollack, E.K., Cadman, T.W., Lee, W.E. and Manning, F.S., "Thermo Properties of Non-Hydrocarbons", H.C. Processing and Petroleum Refiner, Gulf Pub., Houston, TX (January 1966) as in *Engineering Data Book*, Nat. Gas Suppliers Association (1966).
- Chapman, G.T. and Storrs, C.L., *Effective Neutron Removal Cross Sections for Shielding*, U.S. Atomic Energy Comm. AECD-3978 (1955).
- Colston, B.W., "Nuclear Power Supplies: Their Potential and the Practical Problems to their Achievement for Space Missions": In NASA (June 1986), *op cit.*
- Comer, G. "Mars Vehicle TCS and Aeorbrake TPS," *ibid.*

- Criswell, D.R., *Extraterrestrial Materials Processing and Construction*, Final Report, NASA CR-167756 (1980).
- Duke, M. B. and Keaton, P.W., eds., *Manned Mars Missions*, (Working Group Summary Report), NASA M001 (May 1986).
- Duke, M.B., "Mars Resources": in NASA (June 1986), *op cit*.
- Edwards, D.K., Denny, V.E. and Mills, A.F., *Transfer Processes*, McGraw-Hill Book Company, New York, (1976).
- Eckert, E.R.G., in *The Encyclopedia of Physics*, 2nd Ed., R.M. Besancon, ed., Van Nostrand Reinhold, New York (1974).
- Egan, G.J. and Lynch, F.E., "Investigation of Metal Hydrides for Integration of Spacecraft Hydrogen Resources", Final Report for NAS8-35270 (July 1985).
- Ewell, R., "The SP-100 Nuclear Power System": in Noon, E.L., ed. *Proceedings of the 1981 Working Group Meeting on Thermoelectrics*, NASA Jet Propulsion Laboratory, CIT, Pasadena (January 1982).
- French, J.R., "Nuclear Powerplants for Lunar Bases": in Mendell, W.W., ed. *vide infra*.
- French, B.M., *The Moon Book*, Penguin Books, Middlesex, England, (1977).
- Gibson, M.A. and Knudsen, C.W., "Lunar Oxygen Production From Ilmenite" (1984): in Mendell, W.W., ed., *vide infra*.
- Glasstone, S. and Sesonske, A., *Nuclear Reactor Engineering*, 3rd Ed., Van Nostrand Reinhold, New York (1981).
- Gornits, V., ed., *Geology of the Planet Mars*, Benchmark Papers in Geology Series, Dowden, Hutchinson and Ross, Inc., (1979).
- Guidici, R.J., "Electrical Power Systems for Mars," in NASA (June 1986), *op cit*.
- Harless, W., Private Communication, General Electric Co., Sunnyvale CA, (1987).

- Haskin, L.A., "Toward a Spartan Scenario for Use of Lunar Materials" (1985): In Mendell, W.W., ed., *vide infra*.
- Hill, T.L., *An Introduction to Statistical Thermodynamics*, Addison-Wesley, Reading, MA (1960).
- Hirschfelder, J.O., Curtiss, C.F., and Bird, R.B., *Molecular Theory of Gases and Liquids*, 2nd Ed., Wiley & Sons, New York (1964).
- Horz, F., "Lava Tubes: Potential Shelters for Habitats," in Mendell, W.W. ed., *vide infra*.
- Kliore, A., ed., "The Mars Reference Atmosphere," *Advances in Space Research*, Vol. 2, No. 2, Pergamon Press, (1982).
- Kopal, Z., ed., *Physics and Astronomy of the Moon*, Academic Press, New York, (1971).
- Leovy, C. "Martian Meteorological Variability," in "The Mars Reference Atmosphere," *Advances in Space Research*, Vol. 2, No. 2 (1982).
- Lundin, C.E. and Lynch, F.E. "Modification of Hydriding Properties of AB_5 Type Hexagonal Alloys through Manganese Substitution," *Proc. Miami International Conference on Alternative Energy Sources*, University of Miami, (1976).
- Lynch, F.E. and Riter, J.R., "Metal Hydride Properties for Advanced Extravehicular Mobility Unit Heat Pump", Final Report for NAS 9-17549 (March, 1987).
- Martin Marietta Corporation, "E.P.M. Space Practices Engineering Practices Manual", Section S14.0, Thermal Control, (December 1970).
- Mendell, W.W., ed., *Lunar Bases and Space Activities of the 21st Century*, Lunar Space Institute, Houston, (1985).
- Mueller, W.M., Blackledge J.P., and Libowitz, G.G., *Metal Hydrides*, Academic Press, New York (1968).

NASA, "Manned Mars Missions", (Working Group Papers), NASA M002 (June 1986).

NASA, "Space Station Reference Configuration Description," Systems Engineering and Integration Space Station Program Office. JSC-19989, (August 1984).

Owen, T. "The Composition of the Martian Atmosphere": In "The Mars Reference Atmosphere," Advances in Space Research, Vol. 2, No. 2 (1982).

Ozisik, M.N., *Boundary Value Problems of Heat Conduction*, International Textbook Company, Scranton, Pennsylvania (1968).

Rowley, J.C. and Neudecker, J.W., " *In Situ* Rock Melting Applied to Lunar Base Construction and for Exploration Drilling and Coring on the Moon": In Mendell, W.W., ed. *op cit.*

Sadunas, J.A. and Lehtinen, A., "Thermal Management System Options for High Power Space Platforms" AIAA Paper 85-1047 (1985).

Seiff, A. "Post-Viking Models for the Structure of the Summer Atmosphere of Mars": In "The Mars Reference Atmosphere," Advances in Space Research, Vol. 2, No. 2 (1982).

Taylor, S.R., *Lunar Science: A Post-Apollo View*, Pergamon Press, Inc., New York (1975).

Waligora, J.M. and Sedej, M.M., "Physiological and Technological Considerations for Mars Mission Extravehicular Activity": In NASA (June 1986), *op cit.*

Williams, R. J. and Mullins, O., "Enhanced Production of Water From Ilmenite" (abstract): In *Lunar and Planetary Science XIV, Special Session* Lunar and Planetary Institute, Houston (1983).

Williams R.J., McKay D.S., Giles D., Bunch T.E., "Mining and Beneficiation of Lunar Ores" in Space Resources and Space Settlements (J. Billingham, W. Gilbreath, B. Gossett, and B. O'Leary, eds.), NASA SP-428, NASA, Washington (1979).

APPENDIX A

COMPUTER SIMULATION METHODS

The tubular hydride container is sub-divided radially and axially into thin annular rings or "nodes" (A1). Each internal node, containing hydrides, undergoes sensible heat changes and composition changes as quickly as heat transfer and kinetics permit. The changes are iteratively analyzed across a small time step as many times as required to reach a self-consistent set of conditions among the nodes. When this has been accomplished a new time step is taken and the iteration process is repeated.

Nodal analysis of hydrides has been done by others (A2, A3, A4, A5). The very realistic performance of the present model is largely due to an innovation conceived by HCI's programming consultants at Quadrant Scientific, Louisville, Colorado. The concentration change during each time step, ΔT , is computed as the integral of the rate equation over ΔT at the local pressure, temperature and concentration conditions. The model has a realistic level of sophistication and can run on a microcomputer in a reasonable amount of time.

A cutaway of the hydride bed, tube and filter is shown in Figure A-1. For clarity, only five hydride nodes in the radial direction are shown, and water nodes are not included. In actual use, the number of nodes must be at least 12. The axial direction was incorporated for cases where significant heating and cooling of a fluid is desirable. Each node is separated radially by a distance, Δr , and axially by a distance, Δz . The thickness and length of a node's control volume is therefore Δr and Δz , respectively.

Control volumes surrounding each node have homogeneous physical properties, but their temperatures can vary internally in the axial and radial directions. The outermost node shown is the "tube node," which is comprised entirely of the tube material and lies at the tube-fluid interface. The innermost node is the "filter node," which contains hydride material and is located at the hydride-filter interface. It is assumed that there is no heat transfer from the "filter node" to the filter or through either end.

A simplified flow diagram is shown in Figure A-2. The program starts by setting initial nodal conditions to previously specified

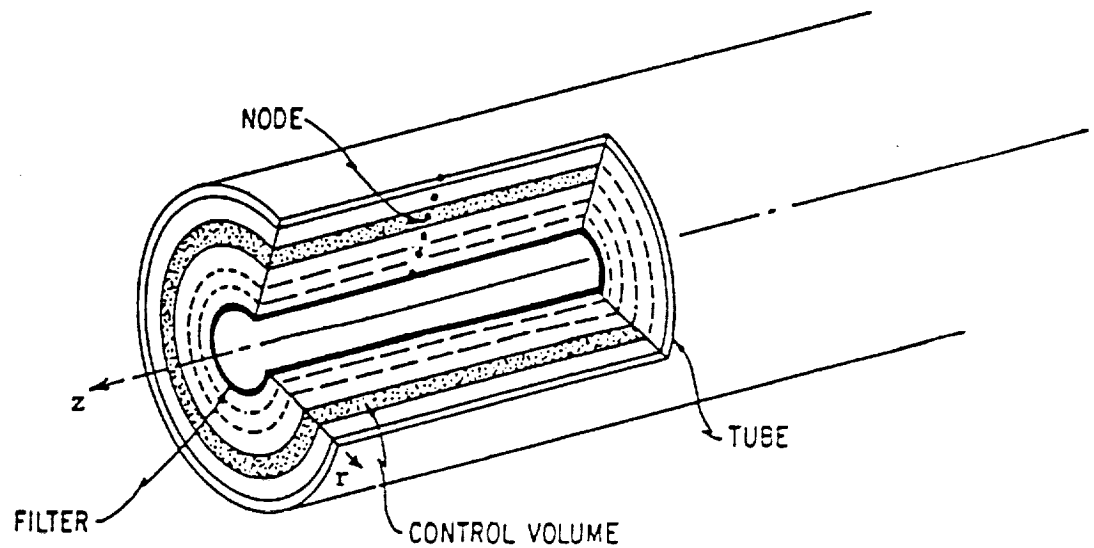


Figure A-1. Cutaway view of the hydride tube model. Each node is a representative point in a control volume Δr thick and Δz long.

temperatures (T_0), concentrations (C_0), bed pressure (P_1) and reaction direction. The main program is then entered, where time (t) is incremented in small steps (Δt).

The main program contains three iteration loops, shown as dashed lines, and one procedural loop shown as a solid line. The innermost iterative loop (*1) adjusts the node temperature (T_{ij}) in order to converge on a solution of the node temperature and composition (C_{ij}). This loop is inside of another (*2) which checks for temperature convergence, typically $\pm 0.025^\circ\text{C}$, and passes program flow only when all equations meet the criteria. These two loops will be discussed in more detail shortly. The outermost loop (*3) adjusts the bed pressure to converge on temperal output (flow or pressure) requirements.

Early in the main program, the heat transfer direction (heating or cooling) and pressure conditions are calculated from their required duty cycles. An example of this would be the cyclic conditions of the MHHP. Next, hydride node conductivity is calculated based on the present concentration (C_{ij}) and bed pressure (P_2).

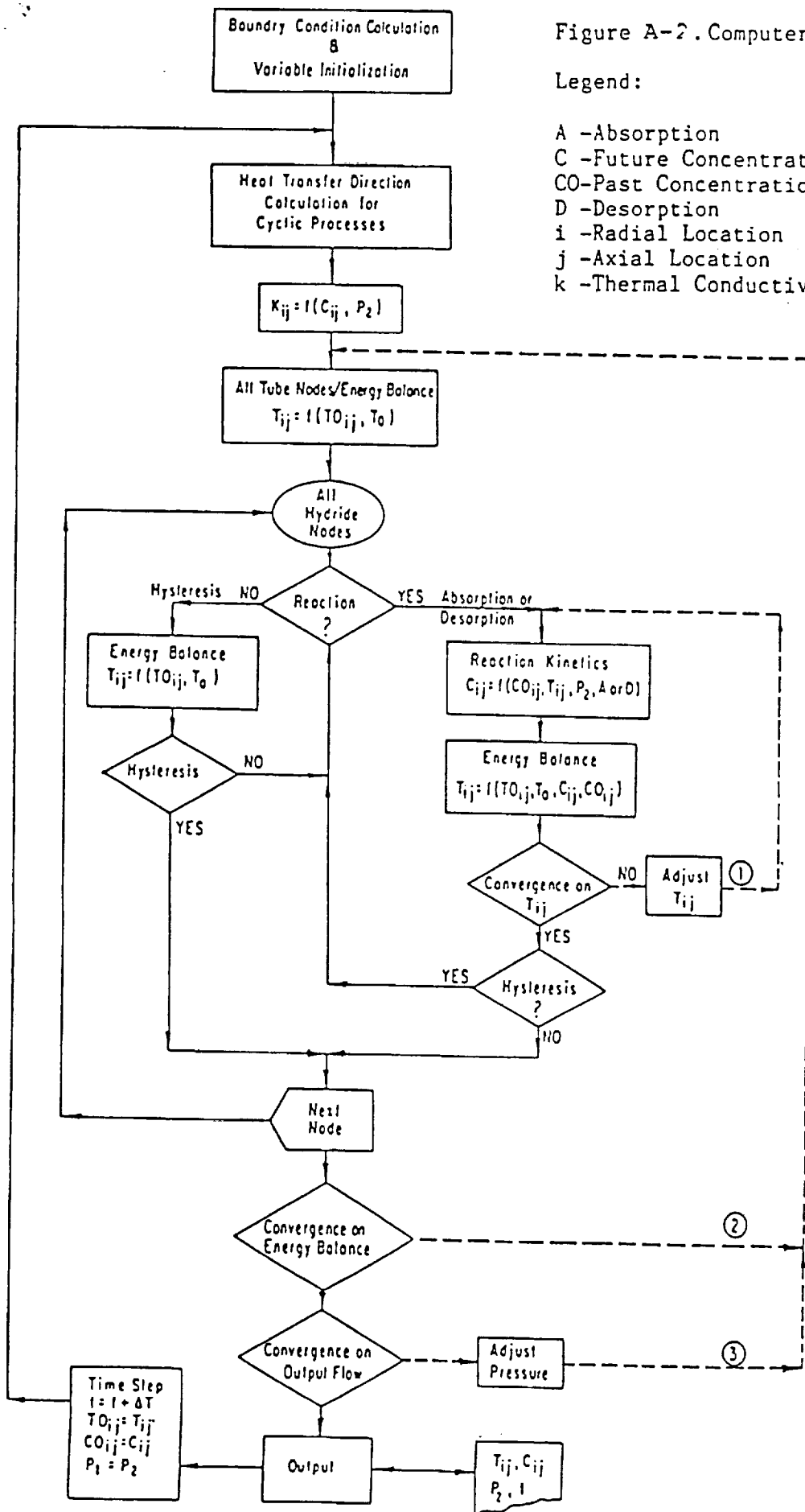


Figure A-2. Computer model flow diagram.

Legend:

A -Absorption	P -Future Pressure
C -Future Concentration	PO-Past Pressure
CO-Past Concentration	T -Future Temp.
D -Desorption	TO-Past Temp.
i -Radial Location	T ^a -Adjacent Node
j -Axial Location	Future Temp.
k -Thermal Conductivity	t - time

Because each hydride node has a "state" condition associated with it, each is treated differently depending on whether it is in desorption, absorption or hysteresis. It is assumed that there is no reaction for nodes in hysteresis. The conditional hysteresis statements, after the hydride nodes energy balance, check for changes in the reaction direction. Thus, any node in the hydride bed may change its "state" as a result of local conditions and subsequently be handled by the proper equations.

Finally, after all equations have converged on solutions, a new time step is taken and old conditions of temperature (T_{Oij}), concentration (CO_{ij}) and pressure (P_1) are set equal to the most recent calculation of T_{ij} , C_{ij} and P_2 .

An energy balance for all nodes was set-up using the implicit formulation of the finite difference equations (A6). The implicit technique is inherently stable and allows time steps and control volume thicknesses (Δr) to be chosen for speed or accuracy, without concern for stability.

This two-dimensional transient system of equations, with internal energy storage and heat sources (or sinks), was solved with an iteration technique that gave swift convergency. This iteration is shown in Figure 20 as loop #2. A modified Liebmann method (A7) was used, where, as soon as a node's new temperature was calculated, it was immediately substituted for the previous one. Thus, new equations in the iteration pattern used more up-to-date temperatures, shortening the iteration process. The iteration technique was further enhanced by using old temperature node profiles for the new "guesses" at the start of a new iteration loop.

A secant method iteration (A8) was used for solving a given node's temperature and composition inside the outer Liebmann iteration. This is shown as loop #1. Convergence of this "inside" iteration was very fast using the previous nodal temperature and the van't Hoff equilibrium temperature as starting points. Three iterations were usually sufficient to get a convergence of better than $\pm 0.025^\circ\text{C}$. This inner iteration eliminated some instabilities, which resulted from expressing the implicit finite difference equations in a convenient algebraic form.

The kinetic rate expression used in the model was similar to El Oseri (A2) and Cummings & Powers (A5) and can be written as:

$$\frac{dC}{dt} \propto K(T) \cdot \frac{P_{eq} - P_2}{P_{eq}} \cdot CO$$

where C and CO = new and old concentration; K(T) = rate constant; P_{eq} = van't Hoff equilibrium pressure at temperature (T); P_2 = applied pressure in the hydride. The rate constant is used in the familiar Arrhenius expression:

$$K(T) = A \cdot e^{-E_a/RT}$$

where E_a = activation energy; R = gas constant; T = temperature; A = constant. The first order rate equation was integrated to improve the accuracy of the concentration calculation compared to average values over large time steps.

A.1 REFERENCES FOR APPENDIX A

- A1 Kranck, J. and Nicolson, P., "A Practical Method for Numerical Evaluation of Solutions of Partial Differential Equations of the Heat Conduction Type", Proc. Cambridge Philosophical Society, Vol. 43, 1947, pp. 60-67.
- A2 El Oseri, I.A., "Theory of the Computer Code RET 1 for the Calculation of Space-Time Dependent Temperature and Composition Properties of Metal Hydride Hydrogen Storage Beds", Int. J. Hydrogen Energy, Vol. 8, No. 3, pp. 191-198, 1983.
- A3 Fisher, P.W. and Watson, J.S., "Modeling and Evaluation of Designs for Solid Hydrogen Storage Beds", Int. J. Hydrogen Energy, Vol. 8, No. 2, pp. 109-119, 1983. (Oak Ridge Natl. Lab. for U.S. DOE cont. W-7405-Eng-26.)
- A4 Podgorny, A.N. et al., "Some Aspects of Metal Hydride Applications as Automotive Hydrogen Storage Units", Hydrogen Energy Progress IV, Proc. 4th World Hydrogen Energy Conference, Pasadena CA, 1982.
- A5 Cummings, D.L. and Powers, G.J., "The Storage of Hydrogen as Metal Hydrides", Ind. & Eng. Chem. Process Des. Develop., Vol. 13, p. 182, April 1974.

A6 Kreith, F., "Principles of Heat Transfer", Intext Educ. Publ., NY NY, 1973. ISBN 0-7002-2422-X, pp. 203-204.

A7 Lapidus, L. "Digital Computation for Chemical Engineers", McGraw-Hill Book Co., NY NY, 1962.

A8 Johnson, L.W. et al., "Numerical Analysis", Addison-Wesley Publ. Co., Reading MA, 1982, pp. 166 ff. ISBN-0-201-10392-3.